THEORY OF PARTICLE DEPOSITION BY INERTIAL FORCES AT BIFURCATIONS IN THE HUMAN RESPIRATORY TRACT

by

Karl A. Bell

Master's Report

Chemical Engineering Laboratory

California Institute of Technology

Pasadena, California

June 2, 1970

Revised October 1, 1970

ABSTRACT

The prediction of lung disease development in man from aerosol particles and the medical justification for subsequent control of particulate atmospheric pollutants requires specific knowledge of the rate and location of the aerosol deposition in the lungs. A theoretical development is presented to numerically predict the rate and location of aerosol deposition by impaction at the wedge walls in a model of a lung bifurcation Two limiting flow cases, steady potential flow and steady laminar boundary layer flow, are analyzed and found to represent upper and lower bounds of limited experimental deposition data for one-micron particles obtained from a lung apparatus simulating normal inhalations.

Numerical deposition results for 20, 10, 5, 4, 3, 2, and 1 micron particles in steady potential flow show deposition fluxes to be functions of Stokes number and also the local air velocity distribution along the wedge. Boundary layer deposition results for the same particles are found to correspond to the first few data points of the steady potential case, however no boundary layer deposition occurs beyond a few particle diameters along the wedge.

TABLE OF CONTENTS

INTRODUCTION

Findeisen[1] in 1935 was the first to develop a theory to quantitatively predict the total deposition of particles in the lungs. In the 1950's Landahl[2] and Beeckmans[3] have followed Findeisen's lead with refinements in the equations for predicting deposition of aerosols by impaction, gravity settlement, and Brownian diffusion in different regions of the respiratory tract.

Their deposition equations are mainly empirical correlations which include the basic theoretical relations for settling velocity, Brownian diffusion, relaxation time, and stopping distance (See Table B3 in the Appendix). The relaxation time and stopping distance are two of the parameters used to characterize the inertial deposition of particles. The stopping distance is the distance a particle travels before coming to rest when it is projected with a given velocity into still air. The relaxation time is the time period required for a particle to adapt its motion to the accelerating or decelerating effect of an externally applied force.

The total deposition in any region of the lung is obtained by summing the separate probabilities for deposition by impaction, settling, and diffusion. As an example of the empirical nature of these deposition equations, Landahl's formula for the probability of inertial deposition is I=P/P+1

where P, the deposition parameter, equals the ratio of the stopping distance to the radius of the bronchial tube. This formula was chosen because it matched the results of an experiment in which 50% deposition occurred at a 90° bend in a pipe when P equaled one! In all cases, plug flow is assumed, or average stream velocities are used. In spite of the obvious simplifications of these equations, they have been useful in predicting gross regional deposition rates in the bronchial tree and the lower respiratory tract.

Specific areas of the lung are initially affected by some lung diseases caused by particle deposition. At these areas the particle deposition rates may tend to be higher, or possibly the natural clearing action of the cilia or phagocytic cells may be less effective. Once the natural form and functions of these susceptible areas are impaired, the disease may spread into surrounding tissue. An example is the case of lung cancer in humans. Primary pulmonary carcinoma in man is considered to be bronchiogenic in origin and usually arised in a principal branch of the main bronchus near the hilus of the lung. It is caused by direct primary contact of carcinogenic vapors or particles (asbestos, arsenic, chromates, nickel carbonyls, tars, and radioactive minerals) on the epithelial lining of the bronchus. The general mechanism for tumor development is believed to be the following: in the bronchial lining a defect caused by the carcinogenic substance is repaired by a transitional type cell which will differentiate normally; however, when persistent injury occurs, they form

cancerous cells.[4]

With today's interest in combating air pollution and in modeling the environment in a manner to optimize the quality of life, man desires to be able to predict statistically the chances of his obtaining lung cancer or some other respiratory disease from breathing polluted air containing various gases and particles. Therefore, he must be able to predict the rates of deposition of specific size particles at specific locations in the lungs. The previously described empirical correlations for regional deposition are inadequate because they neglect local variation in stream velocities and fail to account for the transient momentum and concentration gradients.

Inasmuch as lung cancer develops in the main bronchi and its branches, it is probable that some of the particles contributing to the disease are deposited by inertial forces since the flow rates are high and the streamlines bend significantly at the bifurcation. The bifurcation region is, consequently, the first logical "hot spot" to investigate in the lung.

The goal of this master's report is to theoretically predict the rate and location of the particle deposition at the bifurcation of a lung model and to compare the theoretical results with experimental data taken for a flow system analogous to the first bifurcation in the upper airways.

THEORETICAL ANALYSIS

Lung Model

In nearly all theoretical deposition studies, Weibel's[5] regular symmetric dichotomy model of the lung is used. For the author's theoretical study a two dimensional model of the trachea and its two bronchi with a 90° interbronchial angle and an overall shape identical to Weibel's model is proposed. A sketch of a real lung branching network is shown in Figure 1; the model is shown in Figure 2. The two dimensional model was chosen for study because it simplifies the analytic solution of the streamlines (vorticity effects arise in three dimensions). This simplification should remain accurate for the streamlines close to and on either side of the stagnation streamline. Since gravitational effects are neglected in horizontal flow, only inertial forces are considered. The 90° wedge was chosen because it simplifies the potential and boundary layer solutions. The model is also geometrically similiar to all branching sections in the upper respiratory tract of the lungs; therefore, deposition predictions for this section can be flow rate corrected and applied to any other section.

The main disadvantage is that such a two dimensional symmetric model is not a complete simulation of the three dimensional flows in the real lung. The real lung is unsymmetric with an interbronchial angle which varies from 50 to 100 degrees. The angle seldom is bisected by the trachea, is more rounded, and is not entirely wedge-shaped in three

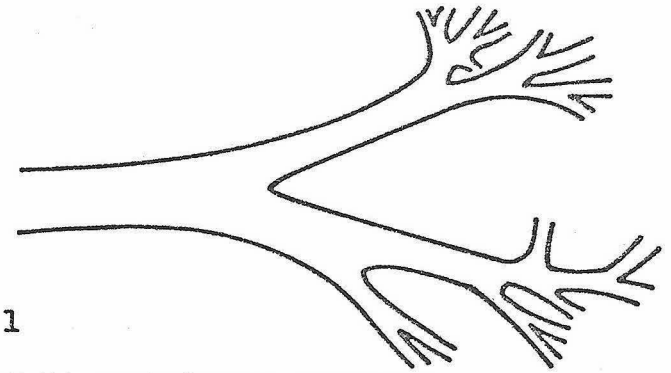

FIG. 1

REAL LUNG BRANCHING NETWORK

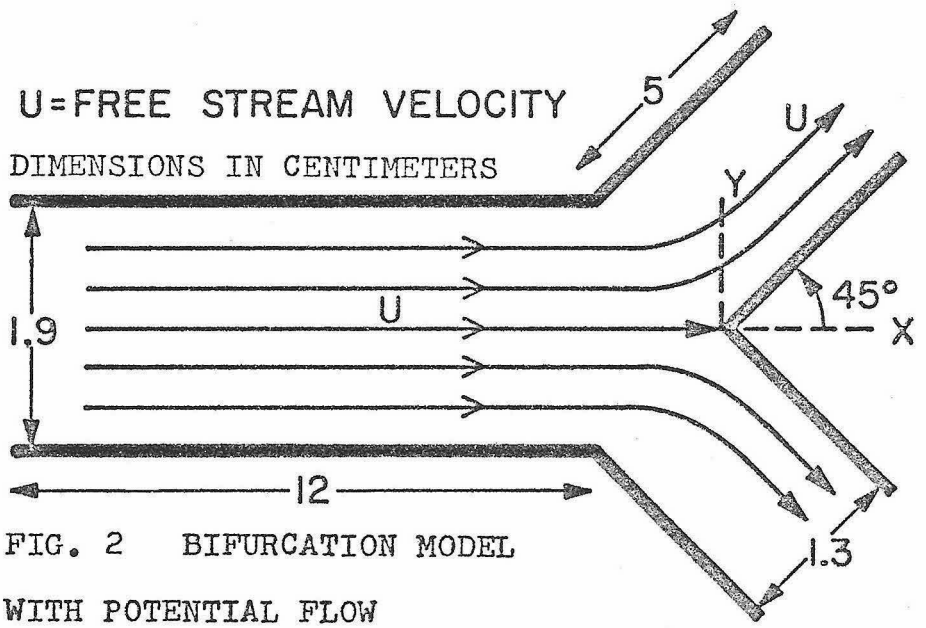

FIG. 2 BIFURCATION MODEL

WITH POTENTIAL FLOW

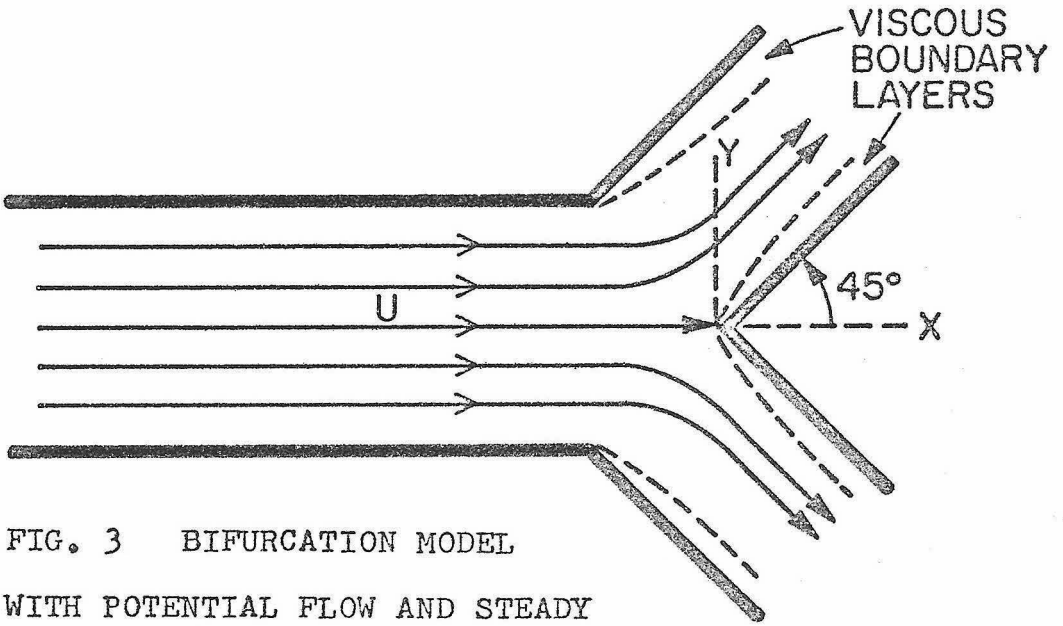

FIG. 3 BIFURCATION MODEL

WITH POTENTIAL FLOW AND STEADY

VISCOUS BOUNDARY LAYERS

dimensions. Finally, the outside walls of the real lung trachea join smoothly with its branches in many possible angles, whereas the model has a sharp 135° angle.

An air flow analysis of Weibel's symmetric lung model is given in Table B1 in the Appendix. The Reynolds numbers and the entrance lengths suggest that laminar plug flow exists in the first through fourth generations, partially developed laminar parabolic flow is present in the fifth through eighth, and well-developed Poiseuille flow takes place in the ninth through fifteenth generations.

For the model studied two flow cases are assumed: (1) steady potential flow shown in Figure 2 and (2) steady potential flow with steady laminar boundary layers in the bifurcation region of Figure 3. In the potential flow solution the infinite velocities at the 135° angle are neglected because the main concern is with the streamlines about the wedge. These cases are simplifications of the real lung flow which is nearly sinusoidal in time and which causes an unsteady boundary layer to develop along the tube walls. However, these cases are valid starting points for a theoretical analysis.

General Streamlines for the Lung Model

Having assumed the two air flow cases, the analytical equations for the steady potential flow will be derived first. Milne-Thomson[6] gives a solution procedure for the general problem of determining the streamlines in a canal with a side branch. Since the flow model proposed above is symmetric, the streamlines can be derived by modifying Milne-Thomson's procedure for either the top or bottom half of the model--the center being determined by the stagnation streamline which terminates at the wedge tip. The top half of the model is shown in the z-plane in Figure 4. The free stream velocity upstream from the branch at A_∞ is U, and the downstream velocity is U_2, unknown. $A_\infty C$ is the stagnation streamline, while the streamline $A_\infty E D_\infty$ undergoes an abrupt change of direction at E, causing an infinite velocity.

First, the branch form in the z-plane is eliminated by transforming into the Q-plane (Figure 4) by the transformation equation

$$Q = \log \frac{U}{\overline{\nu}} = \log \frac{U}{q} + i\theta$$

where $\overline{\nu} = q e^{-i\theta} = u - iv$. Here $q = \sqrt{u^2 + v^2}$, the stream speed. Along the sides of the main canal $\theta = 0$; while along the branch $\theta = \alpha$. At C, $q = 0$; hence, Q is infinite. The infinite strip in the Q-plane can now be mapped into the plane (Figure 4) by means of the Schwarz-Christoffel transformation, which results in the following:

$$\zeta = e^{-Q\pi/\alpha} = -\left(\frac{\overline{\nu}}{U}\right)^{\pi/\alpha} \qquad (1)$$

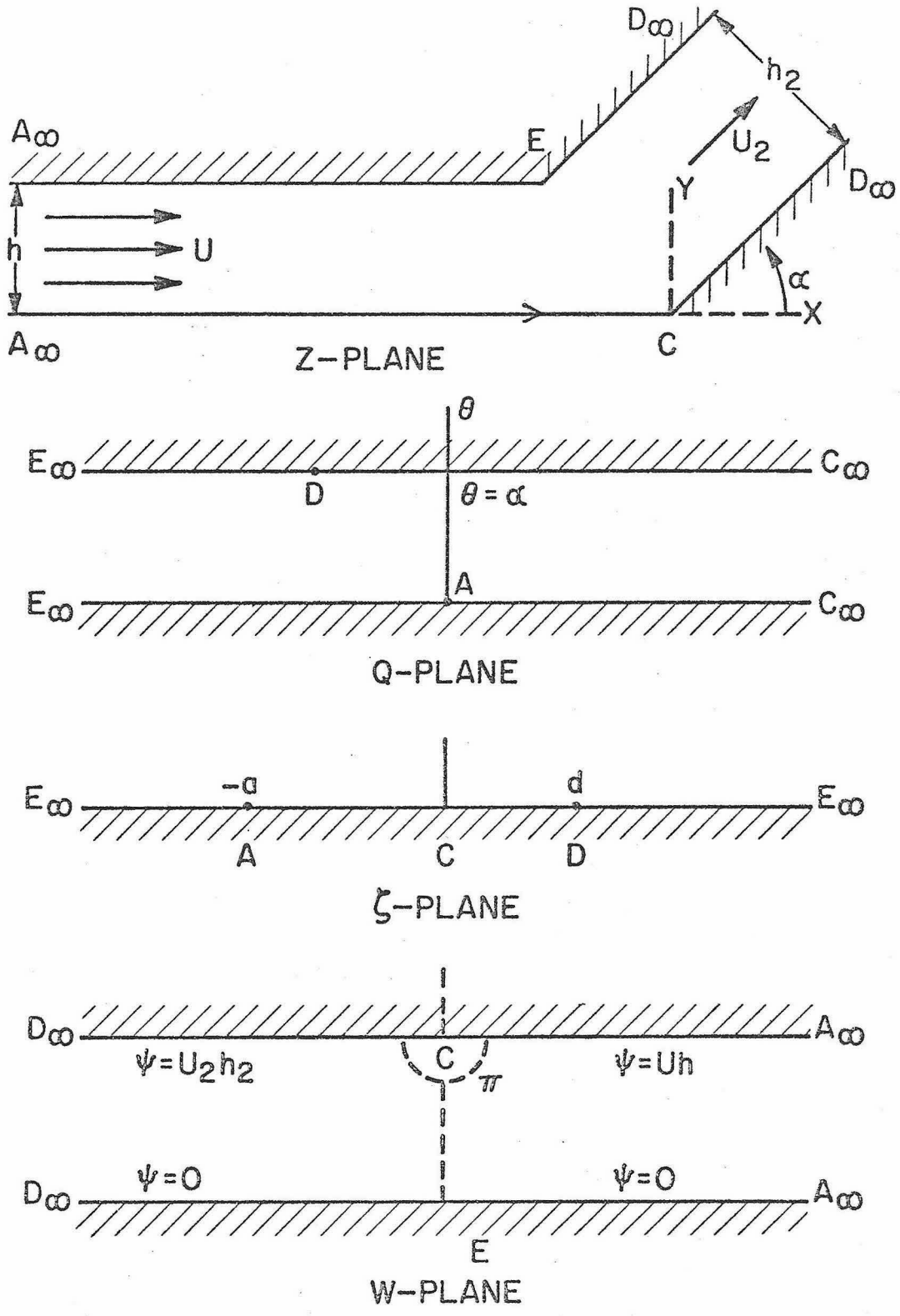
D_∞
h_2
A_∞
E
U_2
Y
D_∞
h
U
α
X
A_∞
C
Z-PLANE
θ
E_∞
C_∞
D
θ = α
A
E_∞
C_∞
Q-PLANE
E_∞
-a
d
E_∞
A
C
D
ζ-PLANE
D_∞
A_∞
$\psi = U_2 h_2$
C
π
$\psi = Uh$
D_∞
$\psi = 0$
$\psi = 0$
A_∞
E
W-PLANE

FIG. 4

The following values of ζ and ν correspond by the above transformation equation:

$$\zeta = -a \qquad \nu = U$$

$$\zeta = d \qquad \nu = U_2 e^{-i\alpha}$$

Therefore, from (1) $a = 1$, and $d = (U_2/U)^{\pi/\alpha}$ (2)

The next step is to construct the complete potential plane or W-plane where $W = \phi + i\psi$. ϕ represents the potential function, while ψ represents the stream function.

Using $\psi = 0$ on $A_\infty E D_\infty$, the boundary conditions are as follows:

on $A_\infty E D_\infty$ $\qquad \psi = 0$

on $A_\infty C$ $\qquad \psi = Uh$

on $C D_\infty$ $\qquad \psi = U_2 h_2$

Therefore,

$$Uh = U_2 h_2 \tag{3}$$

which also follows from the equation of continuity.

Taking $\phi = \infty$ at A_∞, and $\phi = -\infty$ at D_∞, the result is the W-plane diagram shown in Figure 4. To map the W-plane into the ζ-plane, the Schwarz-Christoffel transformation is used again, and the result is the following:

$$\frac{dW}{d\zeta} = K_1 (\zeta + a)^{-1} (\zeta - d)^{-1} = \frac{K_1}{(a+d)} \left[\frac{1}{(\zeta - d)} - \frac{1}{(\zeta + a)} \right]$$

Integrating:

$$W = \frac{K_1}{(a+d)} \log \frac{(\zeta - d)}{(\zeta + a)} + L_1 \tag{4}$$

where K_1 and L_1 are complex constants.

The author's original potential flow derivation was

critically analyzed by Dr. Norman Malmuth and Dr. William Hall.[7] They found that Milne Thomson's derivation and subsequently my previous derivation was in error, because K_1 and L_1 were assumed to be either real or imaginary when applying the boundary conditions to evaluate K_1 and L_1. As indicated above, K_1 and L_1 must both be assumed to be complex constants in order to be evaluated correctly.

Using the boundary condition that $\Psi = 0$ on $D_\infty E$, $(\zeta + a)$ and $(\zeta - d)$ have the same sign. Thus on $D_\infty E$ the logarithms are all real. Therefore on $D_\infty E$

$$\Phi = \frac{Re\, K_1}{(a+d)} \log \left|\frac{\zeta - d}{\zeta + a}\right| + Re\, L_1$$

$$\Psi = 0 = \frac{Im\, K_1}{(a+d)} \log \left|\frac{\zeta - d}{\zeta + a}\right| + Im\, L_1$$

Therefore,

$$Im\, L_1 = \frac{-Im\, K_1}{(a+d)} \log \left|\frac{\zeta - d}{\zeta + a}\right|$$

Evaluating the log in the limit as $Re\,\zeta$ approaches ∞, $\log(1) = 0$. Therefore, $Im\, L_1 = 0$. Thus

$$0 = \frac{-Im\, K_1}{(a+d)} \log \left|\frac{\zeta - d}{\zeta + a}\right|$$

Evaluating the log in the limit as $\zeta \to 0$, $\log\left|\frac{-d}{a}\right| =$ constant; therefore $Im\, K_1 = 0$. Applying the other boundary condition that $\Psi = U_2 h_2$ at C, set $\Phi = 0$ since C is a stagnation point. Thus $\zeta = 0$ at C, and substituting into (4)

$$W = i\, U_2 h_2 = \frac{i\, Re\, K_1\, \pi}{(a+d)} + \frac{i\, Im\, K_1}{(a+d)} \log\left|\frac{d}{a}\right| + i\, Im\, L_1$$

From the results of the first two boundary conditions above, the last two terms equal zero. Rearranging

$$Re\, K_1 = \frac{U_2 h_2 (a+d)}{\pi} = \frac{Uh(a+d)}{\pi} = K_1$$

Using $\phi = 0$,

$$0 = \frac{Re\,K_1}{(a+d)} \log\left|\frac{d}{a}\right| + Re\,L_1 - \pi \frac{Im\,K_1}{0}$$

Therefore

$$Re\,L_1 = -\frac{Uh}{\pi} \log\left|\frac{d}{a}\right| = L_1$$

Substituting these values of L_1 and K_1 into (4) and setting $a = 1$ from (2) the general solution for the complex potential in the symmetric model is the following:

$$W = \frac{Uh}{\pi} \log\left[\frac{\zeta/d - 1}{\zeta + 1}\right] \qquad (4')$$

From (1)
$$\zeta = -\left(\frac{v}{U}\right)^{\pi/\alpha} = \left(\frac{v\,e^{i\alpha}}{U}\right)^{\pi/\alpha}$$

Therefore
$$-\frac{dW}{dz} = v = U e^{-i\alpha} \zeta^{\alpha/\pi} \qquad (5)$$

Differentiating (4') and dividing by (5) the result is

$$\frac{dz}{d\zeta} = \frac{-h}{\pi}\left[\frac{1}{(\zeta - d)} - \frac{1}{(\zeta + 1)}\right] e^{i\alpha}\, \zeta^{-\alpha/\pi}$$

Integrating with respect to ζ with $\alpha = \frac{\pi}{4}$ for the 90° model

$$z = \frac{-h}{\pi} e^{i\pi/4}\left[\int \frac{\zeta^{-1/4}}{\zeta - d}\, d\zeta - \int \frac{\zeta^{-1/4}}{\zeta + 1}\, d\zeta\right]$$

Transforming variables by $\zeta = x^4$, evaluating integrals from tables[8] and substituting $d = (h/h_2)^4$ from (2) and (3) above, the final result is

$$z = x + iy = \frac{\sqrt{2}\,h}{\pi} e^{i\pi/4}\left\{\tfrac{1}{2} \log\left|\frac{\zeta^{1/2} - \sqrt{2}\,\zeta^{1/4} + 1}{\zeta^{1/2} + \sqrt{2}\,\zeta^{1/4} + 1}\right| + \tan^{-1}\left[\frac{\sqrt{2}\,\zeta^{1/4}}{1 - \zeta^{1/2}}\right]\right\} \qquad (6)$$

$$-\frac{h_2}{\pi} e^{i\pi/4}\left\{\log\left|\frac{\zeta^{1/4} - h/h_2}{\zeta^{1/4} + h/h_2}\right| + 2\tan^{-1}\left[\zeta^{1/4}\,\frac{h_2}{h}\right]\right\}$$

Since z = 0 corresponds to $\zeta = 0$ from the transformations in Figure 4, the integration constant C = 0.

Because (6) is not invertible to give $\zeta = f(z)$, one must use both (4') and (6) as the solutions for the complex potential at location z in the z-plane in terms of the implicit variable ζ. The stream function ψ is the complex part of W in terms of ζ at location z in terms of ζ. Likewise, the complex velocity $\nu = u - iv$ is given by (5) in terms of ζ at location z in terms of ζ in (6). Therefore, derivation of an analytical expression giving the stream function or the complex velocity as a direct function of a z-coordinate position is not feasible.

Such a problem should be solvable numerically on a computer. The procedure to determine the stream function, for instance, would be to feed the computer different values of the complex variable ζ and to have it calculate the z coordinates and the value of the stream function ψ corresponding to each value of ζ. Then the computer would sort through this data for all the stream functions of one value and store the (x,y) coordinates of that stream function. In order to plot the streamlines in the z-plane for each value of ψ, the coordinates would be arranged from minimum to maximum based on the x coordinate.

To determine the stream velocity components at any coordinate location in the z-plane, the computer would likewise use different values of ζ to calculate corresponding values of u + iv and x + iy, which would be stored in arrays.

The number of different points in any area of the z-plane is infinite; therefore, one should try to choose values of ζ to obtain values of (x,y) which are equally distributed to the accuracy desired over the range of the z-plane in which one is concerned. Then at any possible point in the range of use on the z-plane, a value of u and v can be found in the stored arrays.

Values of ψ have been computed at various (x,y) coordinates by using the procedure described above. However, preliminary results indicate that the amount of computer time necessary to do an adequate job is presently prohibitive.

In the case of aerosol deposition, the streamlines which lie close to the stagnation streamline are of principle interest because small particles on streamlines far from the stagnation streamline in the direction of the channel walls will never impact on the wedge. This is clearly demonstrated by the fact that the stopping distance of 20 micron particles in a stream having a velocity of 100 cm/sec is only about .087 centimeters in the direction perpendicular to the wedge. Since 20 micron particles are approximately the largest particles to penetrate beyond the nasalpharyngeal chamber, all smaller particles that impact on the wedge will have to travel on streamlines lying within .087 centimeters of the stagnation streamline. Therefore, an approximate solution is desired for the streamlines about the wedge by expanding the general solution about $\zeta = 0$.

Streamlines about the Wedge of the Lunz Model

Expanding the complex potential (4') in an infinite Maclaurin Series for small ζ and neglecting the second and higher order terms, the result is as follows:

$$W \cong \frac{Uh}{\pi}\left[i\pi - \left(\frac{1}{d}+1\right)\zeta + \cdots \right]$$

Therefore,

$$\frac{dW}{d\zeta} \cong \frac{Uh}{\pi}\left[-\left(\frac{1}{d}+1\right) \right]$$

$$\frac{dz}{d\zeta} = \frac{dW/d\zeta}{dW/dz} = \frac{h}{\pi} e^{i\alpha} \zeta^{-\alpha/\pi}\left(\frac{1}{d}+1\right)$$

Integrating with respect to ζ and setting the integration constant equal to zero since $z = 0$ when $\zeta = 0$, the result is

$$z = \frac{h}{\pi} e^{i\alpha} \frac{\zeta^{(-\alpha/\pi+1)}}{\left(\frac{-\alpha}{\pi}+1\right)} \left(\frac{1}{d}+1\right)$$

Choosing $\alpha = \frac{\pi}{4}$, solving for ζ, and substituting for the constants, the equation is as follows:

$$\zeta = \left\{ \frac{3\pi e^{-i\pi/4} z}{4h\left[\left(\frac{h_2}{h}\right)^4+1\right]} \right\}^{4/3}$$

Therefore

$$-\frac{dW}{dz} = U e^{-i\frac{\pi}{4}} \zeta^{1/4} = \frac{U e^{-i\pi/3} z^{1/3}}{\left\{ \frac{4h}{3\pi}\left[\left(\frac{h_2}{h}\right)^4+1\right] \right\}^{1/3}} = u - iv$$

The constant,

$$\frac{U}{\left\{ \frac{4h}{3\pi}\left[\left(\frac{h_2}{h}\right)^4+1\right] \right\}^{1/3}}$$

represents the value of u at $z = -1$ and is designated by U_{-1}.

By use of the approximate equation and substituting for ζ

$$W \cong \frac{Uh}{\pi}\left[i\pi - \left(\frac{1}{d}+1\right)\zeta \right]$$

$$W = -\tfrac{3}{4} U_{-1} e^{-i\pi/3} z^{4/3} + iUh \qquad (7)$$

Using (7) in polar coordinates for flow around a 90° wedge with the origin at the wedge tip and with $r = \sqrt{x^2+y^2}$, $\theta = \arctan y/x$,

$$\phi = -\tfrac{3}{4} U_{-1} r^{4/3} \cos\left(\frac{\pi-4\theta}{3}\right)$$

$$\psi = +\tfrac{3}{4} U_{-1} r^{4/3} \sin\left(\frac{\pi-4\theta}{3}\right) + Uh \qquad (8)$$

$$u = U_{-1} r^{1/3} \cos\left(\frac{\pi-\theta}{3}\right) \qquad (9)$$

$$v = U_{-1} r^{1/3} \sin\left(\frac{\pi-\theta}{3}\right) \qquad (10)$$

(9) shows that the u velocity component decelerates toward the stagnation point and accelerates along the wedge. The v velocity component in (10) is noted to continually increase over the same range. These results are directly applicable to the z-plane since the ζ dependence has been eliminated.

The California Institute of Technology IBM 360 computer was used to plot the streamlines given by (8) about the top half of a 90° wedge shown in Figure E1 in the Appendix. The free stream velocity was taken as 100 cm./sec., which represents the average flow rate of a one second 300 cubic centimeter inhalation through the lung model. U_{-1} is, therefore, equal to 81.97 cm./sec. $\psi = 95$ represents the stagnation streamline or negative x-axis, while $\psi = 93$, $\psi = 91$,....., $\psi = 75$ represent values of the stream functions on the successive streamlines above the negative x-axis. As pointed out earlier the 20 micron particle, the largest particle studied in the subsequent impaction analysis, has a maximum stopping distance, 8.7×10^{-2} centimeters, perpendicular to the wedge. Therefore, the only streamlines needed for the theoretical impaction

analysis will lie under $\psi = 90$. Because the abrupt 135° bend in the channel lies at a distance of 1.3 centimeters perpendicular to the wedge, one can readily assume that the infinite velocities developed there will have no effect on the streamlines close to the wedge. Since the general solution streamlines, if they were obtainable, would have the same shape in the region close to the stagnation streamline and wedge surface, it can be assumed that the approximate solution streamlines are sufficiently accurate for this calculation.

Trajectory Equations

Having obtained equations for the fluid velocity in the model, one must develop a method to apply particles to these streamlines and to determine the rates and locations of their deposition on the wedge wall.

For particles ranging from one micron to 20 microns in diameter in a 100 cm./sec. stream, the particle Reynolds numbers range from .06 to 1.2. Stokes Law, $F_k = 6\pi\mu RU$ is valid for Re up to .1; while at Re = 1, it predicts a drag force which is 10 percent too low. Here F_k is the force associated with the fluid stream movement, μ is the viscosity of the fluid stream, R the particle radius, and U the free stream velocity(100 cm./sec.). In spite of this error with the largest particles, the author will use the following differential equations of motion for particles within the Stokes flow regime:

$$\frac{dU_p}{dt} = \frac{1}{\tau}(U - U_p) \qquad \frac{dV_p}{dt} = \frac{1}{\tau}(V - V_p)$$

u and v are the stream velocity components in the x and y directions, and u_p and v_p are the particle velocity components. τ, the relaxation time of the particle, is equivalent to F_k/mass of particle. The technique for determining the aerosol particle trajectories in curvilinear flow is outlined by Fuchs[9] and consists of dividing the trajectory of the particle into corresponding segments using the approximation for the i-th interval:

$$\frac{du_p}{dt} = \frac{1}{\tau}(u_i - u_p)$$

where u_i is the value of u at the beginning of the interval. Integrating and assuming t = 0 and $u_p = u_{pi}$ gives

$$u_p = u_{pi} + (u_i - u_{pi})(1 - e^{-t/\tau}) \qquad (11)$$

at the end of the interval and integrating again gives the x coordinate of the particle at the end of the interval

$$X = X_i + u_i t + \tau(u_{pi} - u_i)(1 - e^{-t/\tau}) \qquad (12)$$

Calculation of a trajectory in the model will begin at one centimeter before the wedge where the stream velocity is essentially rectilinear and equivalent to the free stream velocity. Therefore, the particle velocity can be assumed equivalent to the stream velocity at this point. Our stream velocities u and v are given by equation (9) and (10) for all points through which the particle can pass. Beginning at x = -1 cm. where $u_p = u$, the trajectory is calculated step by step by use of equations (11) and (12). Obviously, the accuracy will be improved with shorter time intervals for each step in regions close to the wedge where the stream-

lines curve significantly.

Deposition Parameter

Now that the equations for determining the trajectory of the particle have been derived, calculation of the position of the particle will continue until the particle contacts the wedge surface or until it travels beyond 2.5 centimeters along the wedge, in which case it will be considered to follow the fluid streamlines. The general deposition parameter to be measured, F_s/C, is the flux of particles to the wedge surface divided by the concentration of particles in the stream; it has dimensions of cm./sec. This is related to the flux of particles in the main stream, F_o, by the principle of continuity, $F_o dy = F_s dL$, where dL is a small segment of the wedge surface at a point L from the wedge tip. In order to apply this to a finite number of particles colliding with the surface at a finite number of positions, the equation, $dy = \Delta y = y_2 - y_1$, where y_2 and y_1 are the vertical starting coordinates of two identical particles at x = -1 centimeters, is used. These particles impact at L_2 and L_1 on the wedge surface with an average deposition location of $(L_2 + L_1)/2$ and $dL = \Delta L = L_2 - L_1$. Therefore,

$$F_s/C = (F_o \Delta Y)/(C \Delta L) = q \cos\theta (\Delta Y)/(\Delta L)$$

where q is the average speed of the two streamlines at the two starting positions y_2 and y_1 and θ represents the angle between the average velocity vector and the horizontal coordinate. This deposition formula can be used accurately if all particles are started within the same small y distance

of each other. To determine the number of particles depositing in a period of time, multiply F_s/C by the particle concentration in the stream and the period of time of deposition.

Having derived all the necessary theoretical equations, a program was written for use in the IBM 360 computer to determine the deposition rates and locations for aerosol particles in steady potential flow. The Fortran IV program listing is given in Appendix E. The variable inputs are the free stream velocity, particle radius and relaxation time, the y increments between starting positions, and a time interval. 20, 10, 5, 4, 3, 2, and 1 micron diameter particles were run because the 20 micron particle represents approximately the largest particle size which penetrates beyond the nasalpharyngeal passages, whereas the one micron particle is essentially the smallest particle having a relaxation time long enough to impact on the lung walls.

In order to approximate the deposition that occurs in the unsteady flow of a real lung inhalation by using the steady flow computer program, the quasi-steady flow approximation is applied. This approximation holds when the dimensionless parameter $R\sqrt{\omega/\nu}$ is less than 1.0[10]. R represents the radius of the main tube before a bifurcation, ω represents the angular breathing frequency, and ν the kinematic viscosity of air. In other words, the unsteady periodic velocity profile which occurs in the respiratory tract upon inspiration and expiration can be treated as a time succession of steady state velocity profiles when the dimensionless frequency parameter has a value

less than 1.0.

Table B2 in the Appendix shows the variation of the frequency parameter in the upper airways for breathing rates of 12, 16.7, and 30 breaths per minute. The values of the parameter are less than one for the three frequencies used in the 4th generation and proceed to decrease to values of .08-.13 in the 16th generation. In the trachea and the first three generations the value decreases from 4.14 to 1.22 at the 30 BPM rate and from 2.61 to .77 at the 12 BPM rate. The author's bifurcation model has dimensions of the first bifurcation between the trachea and primary bronchi. Since the frequency parameter for the three breathing rates varies from 2.61 to 4.14 in this region, the quasi-steady flow assumption can not be rigorously assumed. However in order to simplify the task of predicting the deposition, quasi- steady flow will be assumed as a first approximation.

The following technique was derived to apply the quasi-steady flow assumption to the author's computer program. The cam design curve, shown in Figure C3, approximates the flow rates for a one second 300 cubic centimeter breath. This has been divided into 16 time intervals, and the average flow rate has been calculated from each interval by standard techniques. Table C1 lists the average flow rates and average stream velocities calculated. Then the above computer program is run for a single particle size repetitively at these different average flow rates. Mean values of the deposition flux are calculated at a fixed location along the wedge by weighting

the deposition flux at that location for each steady flow rate run by the appropriate time interval; all the time weighted values of flux are then summed to give the mean value.

Theoretical Results for Steady Potential Flow

A plot of the trajectories of 20 micron particles in 100 cm./sec. potential flow is shown in Appendix E2. In order for these particles to impact as shown, they are started at x = -1 centimeters, separated vertically by 40 microns, and a time interval of .0001 seconds is used with a relaxation time of .00123 seconds. At the more accurate time interval of .00001 seconds, used in all subsequent results, the maximum extent of impaction for 20 micron particles is 1.5 centimeters downstream of the stagnation point. This result is obtained from a vertical starting position of .024 centimeters, which is slightly more than one-fourth of the stopping distance calculated with 100 cm./sec. flow. These results clearly show that all particles must lie within a few diameters of the stagnation streamline in order to impact on the wedge.

Table B1 lists the relaxation times, stopping distances at 100 cm./sec., and the y starting interval between particles for all the particle diameters run in the results below.

Figure B1 is a plot of log F_s/C vs. log L. The 1, 2, 3, 4, and 5 micron plots are observed to be fairly linear; their nearly constant separation is approximately related to the log of the ratio of their relaxation times or diameters squared. However, one notes increasingly nonlinear regions from the 4 micron to 20 micron particles at locations increasing

respectively from 10^{-3} to 10^{-1} centimeters. One also notes a higher density of deposition points in these regions for the 20 micron and 10 micron particles. One naturally expects the decelerating and accelerating effects of the potential velocities to have the least effect on the 20 micron particle's motion and increasingly greater effect on the smaller particles. Therefore, the 20 micron particles easily traverse the slow velocity, curved streamline region near the tip of the wedge with little deflection to impact directly on the wall. The same can occur for the 10 micron particle, but at a distance four times closer to the tip to insure negligible deflection from its original path before the wedge. This reasoning is carried on closer and closer to the tip for the smaller particles with shorter relaxation times, thus explaining the shift and decrease in size of the nonlinear segments of the plots.

Since the computer program is designed to terminate the trajectories when the center of the particle is less than or equal to the particle radius, the size of the radius causes a small part of the effect described above. If the particle falls beneath the imaginary boundary, the calculation of the exact deposition location is based on the radius.

Figure B2 shows the effect of various potential flow rates on the deposition of one micron particles. The velocity averaged deposition curve marked with crosses is determined by the technique described above to approximate the unsteady flow rate deposition of a 300 cc, one second inhalation. Since it nearly coincides with the 100 cm./sec deposition curve, the

100 cm./sec. steady potential deposition results will be used to approximate unsteady flow results. All the curves have the same shape, indicating that the main effect of varying the velocity for the one micron particles is to change the value of the coefficient of the deposition flux term. Because of the small particle mass and relaxation time, the inertial effects are very small causing the particle to deviate only slightly from the streamlines. Therefore, the nonlinear regions found for the larger particles do not occur for particles smaller than 4 microns. Summarizing, inertial effects cause negligible change in the deposition flux for one micron particles when various stream velocities are used.

Figure B3 for 10 micron particles is analogous to Figure B2. The higher velocity plots clearly show the nonlinear portion explained in the first graph. Higher velocities are naturally expected to emphasize the nonlinear portion while minimal effects occur for the slowest flow rates. This is because the degree of deceleration and acceleration is much smaller than at higher velocities, causing the particles to follow the streamlines more closely. The mean deposition curve to be used for the unsteady flow approximation corresponds approximately with the 114 cm./sec. data instead of the 100 cm./sec. data. This shift in the mean deposition curve is due to the increased inertial effects for the higher flow rate runs which outweigh the effects of the slower runs.

Steady Laminar Boundary Layer

Having solved the inviscid flow case, a steady laminar boundary layer is now added along the wedge to determine its effect on deposition. The potential solution for the flow along the wedge from (9) and (10) is

$$U_b = U_{-1} r^{1/3} = U_{-1} x_b^{1/3}$$

The boundary layer coordinates are x_b and y_b, respectively parallel and perpendicular to the wedge surface. This is used as the limiting velocity above the boundary layer along the wedge.

From Schlichting's[11] dimensionless plots of the velocity distribution in the laminar boundary layer along the 90° wedge, one determines the boundary layer thickness at $u_b/U = .99$ to be

$$\delta(x) = 3.43 \sqrt{\nu_1 / U_{-1}}\, x_b^{1/3} \qquad \left(\nu_1 = \frac{\mu}{\rho}\right)$$

Another approach is to use the displacement thickness[12]

$$\delta^*(x) = .985 \sqrt{\nu_1 / U_{-1}}\, x_b^{1/3}$$

as the boundary layer thickness.

A cubic equation was found to be a poor approximation for the boundary layer velocity profile by the Von Karman Integral Momentum Equation. Therefore after applying Schlichting's dimensionless parameters a series expansion of the velocity profile for the 90° wedge was obtained from the original article of Falkner and Skan[13]. The components of the velocity in the boundary layer are therefore:

$$u_b = U_{-1}\left[.8\left(\frac{U_{-1}}{\nu_1}\right)^{1/2} y_b - .166\left(\frac{U_{-1}}{\nu_1}\right) y_b^2 x_b^{-1/3} + .00148\left(\frac{U_{-1}}{\nu_1}\right)^{5/2} y_b^5 x_b^{-4/3}\right]$$

$$v_b = (\nu_1 U_{-1})^{1/2}\left[-.018\left(\frac{U_{-1}}{\nu_1}\right)^{3/2} y_b^3 x_b^{-4/3} + .000328\left(\frac{U_{-1}}{\nu_1}\right)^{3} y_b^6 x_b^{-7/3}\right]$$

In order to determine the deposition rates with the steady laminar boundary layer, the same basic computer program is used as in the steady potential flow case. However, the boundary layer thickness is applied as a boundary condition for switching the particles from the potential flow equations of motion to the equations of motion based on the boundary layer velocity components. The same deposition parameters are used. The Fortran IV program listing is given in Appendix I The displacement thickness was used to obtain the reported data below because the other boundary layer thickness equation gave essentially identical results for all particle sizes. The difference between results was negligible because all sizes of particles which deposited on the wedge entered the boundary layer well within the maximum thickness predicted by the displacement thickness equation.

Boundary Layer Results

Figure B4 is a plot of the deposition results for all particles in a 100 cm./sec. potential velocity stream with a steady viscous boundary layer on the wedge. As one would expect, the slow viscous boundary layer tends to quickly dissipate the momentum of all particles entering it. Only the large 20 micron particle is capable of penetrating and depositing at a maximum distance of .1 centimeters from the wedge tip. The 10 micron particles almost reach .01 centimeter and the remainder of the particles are all deposited within a distance equivalent to their diameter from the wedge tip. The curved tails connect the first deposition value along

the wedge with a theoretical deposition value at the wedge tip, evaluated with $L = 10^{-6}$ centimeters. Deposition plots within 10^{-4} centimeters of the tip are theoretically possible but realistically meaningless when dealing with particles larger than 10^{-4} centimeters. The plots for 2, 3, and 4 microns dip before taining off because the average deposition location is bases on a deposition at L = 0 and L = twice the average location.

Comparisons of this graph with the steady flow case of Figure B1 show that the boundary layer plots roughly approximate the first deposition points of the steady flow case for the 4 micron and larger particles.

Figure B5 represents the steady boundary layer thickness for different steady potential velocities. The thinner boundary layer at 167.5 cm./sec. indicates that more deposition will be possible than at 100 cm./sec. but that the thicker 22.9 cm./sec. case will further hinder deposition.

Figure B6 shows the effect of high flow rates on the deposition of one micron particles when a steady laminar boundary layer is imposed along the wedge. 128.5 cm./sec. was the lowest velocity used in which at least 3 deposition points occurred at the wedge. However, all the deposition points for all the curves are still within one micron of the tip. The inaccuracy of the technique for computing the trajectories and the invalidity of the boundary layer equation at L = 0 make analysis of these separate curves meaningless. However, the general plateau with sharp tail is similar to

the boundary layer results for larger particles. The dotted lines indicate a higher theoretical deposition value at L = 0 and then a sharp dip for the reason explained in the last paragraph.

Figure B7 shows the effect of various steady flow rates on the boundary layer deposition of 10 micron particles. The general trends of higher deposition flux with greater maximum deposition locations at high velocities clearly holds. Comparison of Figure B7 with Figure B3 clearly shows that the shape and location of the boundary layer deposition curve coincides closely with the sections of the 10 micron potential deposition curve to the left of 10^{-2} centimeters from the wedge tip. This shows that as the stream velocity increases, the boundary layer thickness decreases and the inertial forces on the particle increase; therefore, this causes penetration of the boundary layer and impaction at increasingly greater distances along the wedge. The 22.9 cm./sec. curve has an erratic shape because financial limitations prohibit the excess of computer time needed to use a very small time interval in the calculations. The longer time interval results in a less smooth trajectory and subsequently an erratic deposition pattern.

Friedlander's Boundary Layer Solution

Friedlander[14] has suggested an analytical solution to deposition by impaction at a 90° wedge with steady viscous boundary layer. His corrected derivation with some of the author's modifications to account for the particle radius is

given in Appendix D.

Friedlander's solution assumes that the flow in the boundary layer is rectilinear along the wedge -- which is a valid assumption because the value of the perpendicular velocity component from the author's equation is only 10^{-5} cm./sec. Thus, Friedlander makes the approximation of a steady laminar boundary layer.

However, he then assumes that a particle entering the boundary layer will follow the streamlines along the wedge and only have an inertial effect perpendicular to the wall. This will cause the particles to deposit on the wall only if they entered the boundary layer at a distance within the stopping distance plus the radius of the particle. The stopping distance would be evaluated from the potential velocity at the last position before entering the boundary layer. The displacement along the wedge would then be dependent on the velocity of the boundary layer and a fraction of the relaxation time.

Obviously, this solution will predict deposition locations even closer to the wedge tip than the author's results. Since the same relaxation time principles operate as in the perpendicular direction to damp the particle velocity, one cannot instantly neglect the inertial forces in the x_b direction of a particle entering a boundary layer.

The boundary layer computer program in this study was modified to calculate the F_s/C and deposition location by Friedlander's solution for all particles breaking the $x_b = 0$

plane which were within the stopping distance plus the radius of the particle from the wedge surface.

Figure B8 is a comparison plot of Friedlander's analytic boundary layer solution for one micron particles at 167.5 and 100 cm./sec. with the author's numerical boundary layer solution at 167.5 and 128.5 cm./sec. Comparison of plots shows clearly that the previous arguments are correct. The analytic plots have all deposition within 10^{-7} to 10^{-6} centimeters compared to 10^{-5} to 10^{-4} centimeters for the author's data. As expected the analytic deposition fluxes were much higher closer to the tip.

Figure B9 compares Friedlander's analytic boundary layer solution results for 10 micron particles at 100 cm./sec. with the author's numerical boundary layer results. In this case the regions of deposition overlap significantly, however the author's results still show deposition further along the wedge. The deposition fluxes differ by one to two orders of magnitude. The apparent increase of flux with distance along the wedge for the analytic case is puzzling at the present time. It is apparently due to the assumption of no inertial effects in the direction parallel to the wedge wall.

COMPARISON OF THEORETICAL RESULTS WITH EXPERIMENTAL RESULTS

Experimental Procedure

Richard Vincent, an undergraduate student working for Professor Friedlander at the California Institute of Technology has collected experimental data for the deposition of 1.099 micron hydrosol particles made of Dow Polystyrene Latex in the lung bifurcation model shown in Figure C1. A schematic of the experimental apparatus is shown in Figure C2. The cam was designed to simulate a one second 300 cc breath shown in Figure C3.

Vincent collected data for 1.0, 1.8, and 2.5 second 300 cc tidal volume breaths by the following procedure. The holding chamber and piston assembly were flushed with aerosols until the concentration registered about 1.5×10^4 particles/cm.^{3} on a Sinclair-Phoenix Aerosol, Smoke, and Dust Photometer. The chamber was then isolated, the gate lifted, and the cam-driven piston set in motion. At the end of the stroke the gate was lowered, and the test section was flushed gently with ambient air. This procedure was repeated 30 times to allow sufficient deposition on the glass slides for statistically meaningful counts. All singlet particles were counted in an area .0154 inches wide and one inch long under a microscope at 675 magnification.

Analysis of Data

Figures B10, B11, and B12 are comparison plots of the author's steady potential flow data for one micron particles at flow rates of 100, 53.7, and 41 cm./sec. respectively with Vincent's average experimental data for 1.0, 1.8, and 2.5 second 300 cc breaths. These flow rates correspond to the average flow rate in the lung model for the respective breaths. The author's data predict higher deposition rates at all locations. On each graph the initial experimental data point at .024 centimeters has a deposition flux/concentration value 5 to 8.5 times smaller than the authors predicted potential results. The remaining points are 1 to 5 times smaller than the author's predictions. The two longer breath simulations give better agreement between theoretical and experimental data than the one second breath. Since all boundary layer deposition terminates beyond 10^{-4} centimeters, comparison of experimental data with the one micron steady boundary layer results of Figure B4 and B6 is impossible.

The steady potential theory tends to predict deposition values slightly above the experimental results, however the viscous boundary layer theory predicts deposition values far below the experimental results. These relative results for inertial impaction on a wedge generally agree with the results of inertial impaction studies on cylinders and spheres presented by Fuchs.[15] In the cylinder and sphere cases the experimental data is scattered around the steady potential flow curves, while the viscous flow curve predicts much lower

deposition. The experimental data of Walton and Woolcock[16] for the collection efficiency for aerosols on spherical water drops is shown to be parallel to and slightly below the theoretical potential flow curve and well above the theoretical viscous flow curve.

The main weakness of the theoretical simulation of deposition with inhalation has been the steady state assumptions. In the real lung the sinusoidal breathing pattern sets up a thin unsteady boundary layer which never attains the steady state thickness assumed close to the wedge tip. However, even a thin unsteady boundary layer will represent some resistance to particle deposition from the potential flow streamlines. It is logical that the unsteady boundary layer case will theoretically predict deposition values which are slightly lower than the potential flow case, resulting in better agreement with the experimental data.

Data Fitting With Stokes Number

The use of dimensionless parameters to correlate deposition data is a standard practice. Both the experimental and the numerical calculations can be represented by an equation of the form $F_s/C = AL^{-B}$. In general the deposition data in the bifurcation model would be expected to be a function of Stokes number, Reynolds number, and a parameter describing the periodic nature of the flow ($R\sqrt{\omega/\nu}$). Stokes number = $Stk_x = U\rho_p d_p^2/18\mu X$

It is instructive to study the possibility of using only the Stokes number to correlate the data. Figures B13 and B14 are plots of the Stokes number at x distances along the wedge

for one and 10 micron particles and 100 cm./sec. steady potential flow. Plots of the theoretical potential data and experimental data for one micron particles are shown for comparison. Fitting Stokes number to the theoretical data for one micron particles gives the following:

$$F_s/CU = 5.275 \times 10^{-3} (StK_x)^{.7}$$

Fitting Stokes number to the straight line drawn through the experimental data gives the following:

$$F_s/CU = 1.68 \times 10^{-4} (StK_x)^{.44}$$

Following the same procedure in B14 for the 10 micron particles at 100 cm./sec. gives the following:

$$F_s/CU = 9.8 \times 10^{-3} (StK_x)^{1.0}$$

This is a straight line approximation of the 10 micron data on log log coordinates. Because of the actual nonlinear form of the 10 micron data, it is impossible to fit the one and 10 micron data with the same function of the Stokes number. This is understandable since the Stokes number has no mechanism to account for variations in the potential velocity around the wedge. As described earlier these accelerating and decelerating fluid motions cause great differences in the deposition behavior of 1 and 10 micron particles. A local particle Reynolds number may handle this situation($Re_p = U_{loc}\rho_p d_p/\mu$).

SUMMARY AND CONCLUSIONS

Since many lung diseases are known to arise from particle deposition in the bronchial tubes, the first lung bifurcation between the trachea and its two bronchial tubes is a logical "hot spot" to analyze to determine specific tissue doses.

A two dimensional bifurcation model with a 90° wedge was chosen for analysis. The unsteady flow behavior of a real lung was approximated by two steady state flow cases:

(1) steady potential flow

(2) steady potential flow with a steady laminar boundary layer along the bifurcation wedge.

Using the principles of theoretical hydrodynamics, a potential flow solution was obtained for the model. To facilitate numerical calculations of particle trajectories, an approximate analytic potential solution was obtained about the wedge. A solution for the thickness and velocity distribution of the steady laminar boundary layer along the wedge was also obtained. Applying the flow solutions to the differential equation of motion for particles in the Stokes regime, computer runs were made to numerically predict the rates and location of particle deposition along the wedge of the bifurcation.

The numerical deposition results for 20, 10, 5, 4, 3, 2, and 1 micron particles in steady potential flow predict the deposition at a maximum distance of 2.0 centimeters, predict the deposition flux/concentration decreasing as a function

of a negative power of the distance along the wedge, and show that the exact functional form of the data varies for each particle size. Deposition results for large particles are observed to always be higher than for small particles due to their larger relaxation times. Steady boundary layer deposition is only observed to be significant for 10 and 20 micron particles out to a maximum distance of 10^{-2} and 10^{-1} centimeters from the wedge respectively. The smaller particles all deposit within a distance equivalent to their particle diameter from the tip. Increasingly nonlinear convex regions for increasing particle size in the potential flow case is explained by the combination effects of particle relaxation time and the degree of deceleration and acceleration of the stream velocities in the region of particle travel. The nonlinearity also explains the failure of the Stokes number correlation to fit all particle size and flow rate cases.

When compared with experimental data, numerical deposition results for one micron particles in 1.0, 1.8, and 2.5 second simulated inhalations of 300 cc showed that the steady potential case over-estimates the degree of experimental deposition by 5 to 8.5 times at the wedge tip and from 1 to 5 times beyond the tip. However, the one micron steady boundary layer results predict no deposition for potential velocities below 128.5 cm./sec. and no deposition beyond 10^{-4} centimeters for potential velocities at and above 128.5 cm./sec. Our theoretical results represent upper and lower bounds to the unsteady experimental data, therefore a theoretical analysis based on unsteady main stream flow with unsteady boundary layers should give deposition

predictions closer in agreement with experimental data for the model used.

The author plans to continue this research by analyzing the unsteady flow problem, and by collecting more experimental data on various particles sizes. The effect of radial and convective diffusion in the deposition of particles of .1 to .5 micron diameter (size of cigarette smoke particles) at the bifurcation will be studied theoretically, and experimental data collection will be attempted.

ACKNOWLEDGMENTS

The author is very grateful for the advice and continued support provided by Dr. G. M. Hidy, Professor Lester Lees, and Professor S. K. Friedlander.

The author is also indebted to the suggestions given by Dr. william Hall and Dr. Norman Malmuth of the North American Rockwell Science Center upon critical review of the potential flow derivation for the lung model.

This research has been supported financially by a National Science Foundation Traineeship and computation funds from the Environmental Health and Engineering Department of the California Institue of Technology.

This report is presented in fulfillment of the thesis requirements for the degree of Master of Science in Chemical Engineering from the Division of Chemistry and Chemical Engineering, California Institute of Technology.

REFERENCES

1. Findeisen, W. "Über das Absetzen Kleiner, in der Luft suspendierten Teilchen in der menschilichen Lunge bei der Atmun." Pflüger Arch. f.d. ges. Physiol. 236:367, 1935.

2. Landahl, H.D. "On the Removal of Air-borne Droplets by the Human Respiratory Tract: I. The Lung," Bulletin of Mathematical Biophysics, 12:43, 1950.

3. Beeckmans, J.M. "The Deposition of Aerosols in the Respiratory Tract: I. Mathematical Analysis and Comparison with Experimental Data," Canadian Journal of Physiology and Pharmacology, 43:157, 1965.

4. Homburger, Freddy (ed.). Physiopathology of Cancer. Second Edition. New York: Hoeber and Harper, 1959, 32-33.

5. Weibel, E.R. Morphometry of the Human Lung. New York: Academic Press, 1963.

6. Milne-Thomson, L.M. Theoretical Hydrodynamics. New York: Academic Press, 1963.

7. Hall, William and Malmuth, Norman. personal communication, June 1970.

8. Dwight, H.B. Tables of Integrals and Other Mathematical Data. New York: Macmillan Company, 1951, Equation 170.2.

9. Fuchs, N.A. Mechanics of Aerosols. New York: Macmillan, 1964, 135.

10. Womersley, J.R. "Method for the Calculation of Velocity, Rate of Flow and Viscous Drag in Arteries when the Pressure Gradient is Known," Journal of Physiology, 127:553, 1955.

11. Schlichting, H. Boundary Layer Theory. Fourth Edition. New York: McGraw-Hill, 1960, 128-129.

12. Lagerstrom, R. "Solution of Boundary Layer Equations", High Speed Aerodynamics and Jet Propulsion: Theory of Laminar Flows. F.K. Moore (ed.), Princeton, N.J.: Princeton Univ. Press, 1964, IV: 121.

13. Falkner, V.M. and Skan, S.W. Philosophical Magazine. S.7, No. 80, 12: 865-873, 1930.

REFERENCES (cont.)

14. Friedlander, S.K. "A Model for Deposition by Impaction at Lung Branches." Unpublished research, California Institute of Technology, Pasadena, 1970.

15. Fuchs, N.A., op. cit., 76.

16. Walton, W.H. and Woolcock, A. "The Suppression of Airborne Dust by Water Spray," Aerodynamic Capture of Particles. New York: Pergammon Press, 1960, 140.

NOMENCLATURE

Arabic Symbols

c	concentration of particles in stream, particles/cm^3
d_p	particle diameter, cm.
F_o	particle flux in main stream, particles/ cm^2sec
F_s	particle deposition flux on wedge, particles/cm^2sec
h	breadth of main channel in model, cm
h_2	breadth of branch in model, cm
h_s	stopping distance, cm
L	distance along wedge, cm
q	stream speed, cm/sec
Q	transformation variable
t	length of time interval, sec
u,v	x,y directional components of stream velocity in z-plane
u_b, v_b	boundary layer velocities parallel and perpendicular to the wedge
U	main stream velocity at infinite distance before wedge
U_2	branch stream velocity infinite distance beyond wedge
U_{-1}	potential velocity at x= -1 cm before wedge tip
W	complex potential

Greek Symbols

α	bisected wedge angle
$\delta(x)$	boundary layer thickness, cm
Θ	arctan(v/u)
ρ	density of air, gm/cc
ρ_p	density of particle, gm/cc
ϕ	potential function
ψ	stream function
τ	relaxation time of particle, sec
μ	viscosity of air, gm/cmsec
ν	complex velocity cm/sec
ν_1	kinematic viscosity of air, cm^2/sec
ζ	transformation variable
$\delta^*(x)$	displacement thickness, cm
ω	angular frequency of breathing = $2\pi f$, sec^{-1}

TABLE B1

Values of the Reynolds number and the ratio of entrance length to the length of the generation for the upper respiratory tract based on the dimensions of Lung Model A proposed by Weibel[5]. Time of respiration = 4 sec., tidal volume = 450 c.c. The airflow curve is assumed to be sinusoidal.

Gen z	Number N_z	Diam (cm) d_z	Length (cm) l_z	Maximum velocity (cm/sec) $\dot{V}_z$	Reynolds number $N_{Re} = \frac{d_z \dot{V}_z}{\nu}$	Entrance Length / Total Length $\frac{0.55 + 0.056\ Re}{l_z/d_z}$
* 0	1	1.8	12.0	139	1670	-
** 1	2	1.22	4.76	151	1220	17.37
2	4	0.83	1.90	166	913	22.40
3	8	0.56	0.76	176	656	27.44
4	16	0.45	1.27	142.3	427	8.80
5	32	0.35	1.07	113.4	265	5.05
6	64	0.28	0.90	89.1	166	3.06
7	128	0.23	0.76	69.2	106	1.95
8	256	0.186	0.64	50.9	63	1.20
9	512	0.154	0.54	36.9	37.8	0.76
10	1024	0.130	0.46	26.4	22.9	0.52
11	2048	0.109	0.39	18.0	13.1	0.36
12	4096	0.095	0.33	12.2	7.72	0.30
13	8192	0.082	0.27	7.94	4.33	0.25
14	16384	0.074	0.23	5.10	2.51	0.23
15	32768	0.066	0.20	3.12	1.37	0.23
16	65536	0.060	0.165	1.96	0.78	0.22

* trachea

** main bronchus

TABLE B2

This table shows the variation of the dimensionless frequency parameter, $R\sqrt{\omega/\nu_1}$ for various breathing rates in the upper respiratory tract. R = generation radius, cm., $\omega = 2\pi f$, f = breathing rate, $sec.^{-1}$, ν_1 = kinematic viscosity of air = 1.66×10^{-1} $cm.^2/sec.$ at $98.6^{\circ}F$.

Gen	Radius	$R(\omega/\nu_1)^{\frac{1}{2}}$ 12 BPM	16.7 BPM	30 BPM
*0	0.95	2.61	3.08	4.14
**1	0.61	1.68	1.98	2.66
2	0.415	1.14	1.348	1.80
3	0.28	0.77	0.91	1.22
4	0.225	0.62	0.733	0.979
5	0.175	0.4815	0.57	0.763
6	0.14	0.386	0.50	0.61
7	0.115	0.316	0.374	0.501
8	0.093	0.256	0.302	0.404
9	0.077	0.212	0.236	0.335
10	0.065	0.179	0.21	0.282
11	0.0545	0.15	0.177	0.237
12	0.0475	0.13	0.154	0.206
13	0.041	0.113	0.133	0.1785
14	0.037	0.102	0.120	0.161
15	0.033	0.0907	0.107	0.1435
16	0.030	0.0825	0.0974	0.131

* trachea

** main bronchus

12 BPM = 2.5 sec. inhalation, f = .2/sec.

16.7 BPM = 1.8 sec. inhalation, f = .278/sec.

30 BPM = 1.0 sec. inhalation, f = .5/sec.

TABLE B3

PARTICLE PARAMETERS

Diameter-d_p microns	Diameter-d_p cm	Relaxation Time τ sec	Stopping Distance h_s sec	Δy cm
20	$2X10^{-3}$	$1.23X10^{-3}$	$8.70X10^{-2}$	$2X10^{-3}$
10	$1X10^{-3}$	$3.08X10^{-4}$	$2.18X10^{-2}$	$2X10^{-4}$
5	$5X10^{-4}$	$7.70X10^{-5}$	$5.45X10^{-3}$	$5X10^{-5}$
4	$4X10^{-4}$	$5.03X10^{-5}$	$3.56X10^{-3}$	$4X10^{-5}$
3	$3X10^{-4}$	$2.70X10^{-5}$	$1.91X10^{-3}$	$3X10^{-5}$
2	$2X10^{-4}$	$1.31X10^{-5}$	$9.25X10^{-4}$	$1X10^{-5}$
1	$1X10^{-4}$	$3.54X10^{-6}$	$2.54X10^{-4}$	$4X10^{-6}$

$\tau = \rho_p d_p^2 / 18\mu$

$h_s = V \sin\theta \tau$ V = 100 cm/sec $\theta = 45^\circ$

Δy = vertical separation between particles at starting position for each trajectory run

Note: A time interval of .00001 seconds was used in all steady potential runs; a second time interval of .00001 or .00002 seconds was used inside of the boundary layer.

A particle at rest acquires 1/e of the velocity of a suddenly applied air stream in τ seconds.

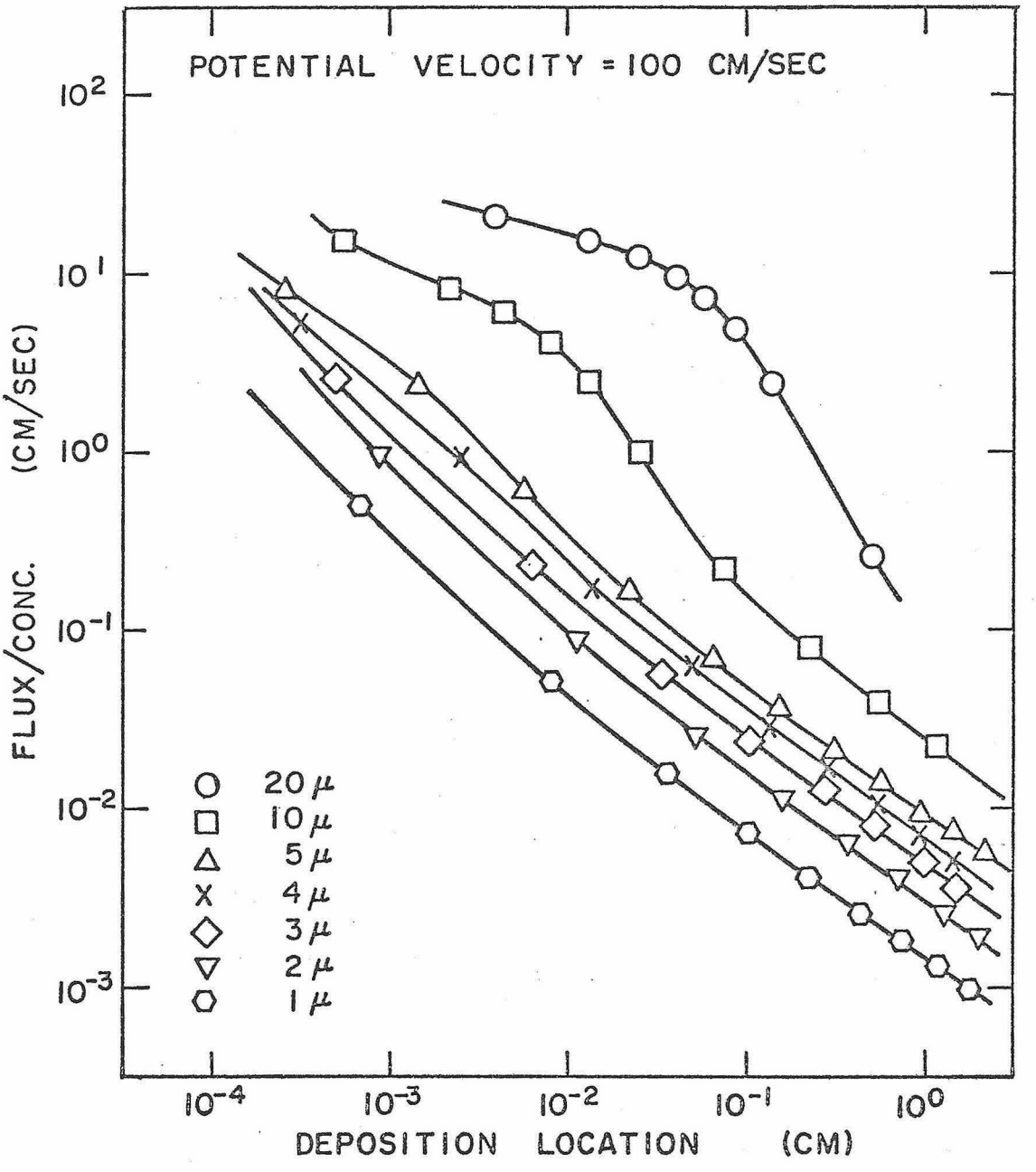

FIG. B1 STEADY POTENTIAL FLOW DEPOSITION CURVES FOR VARIOUS PARTICLE SIZES

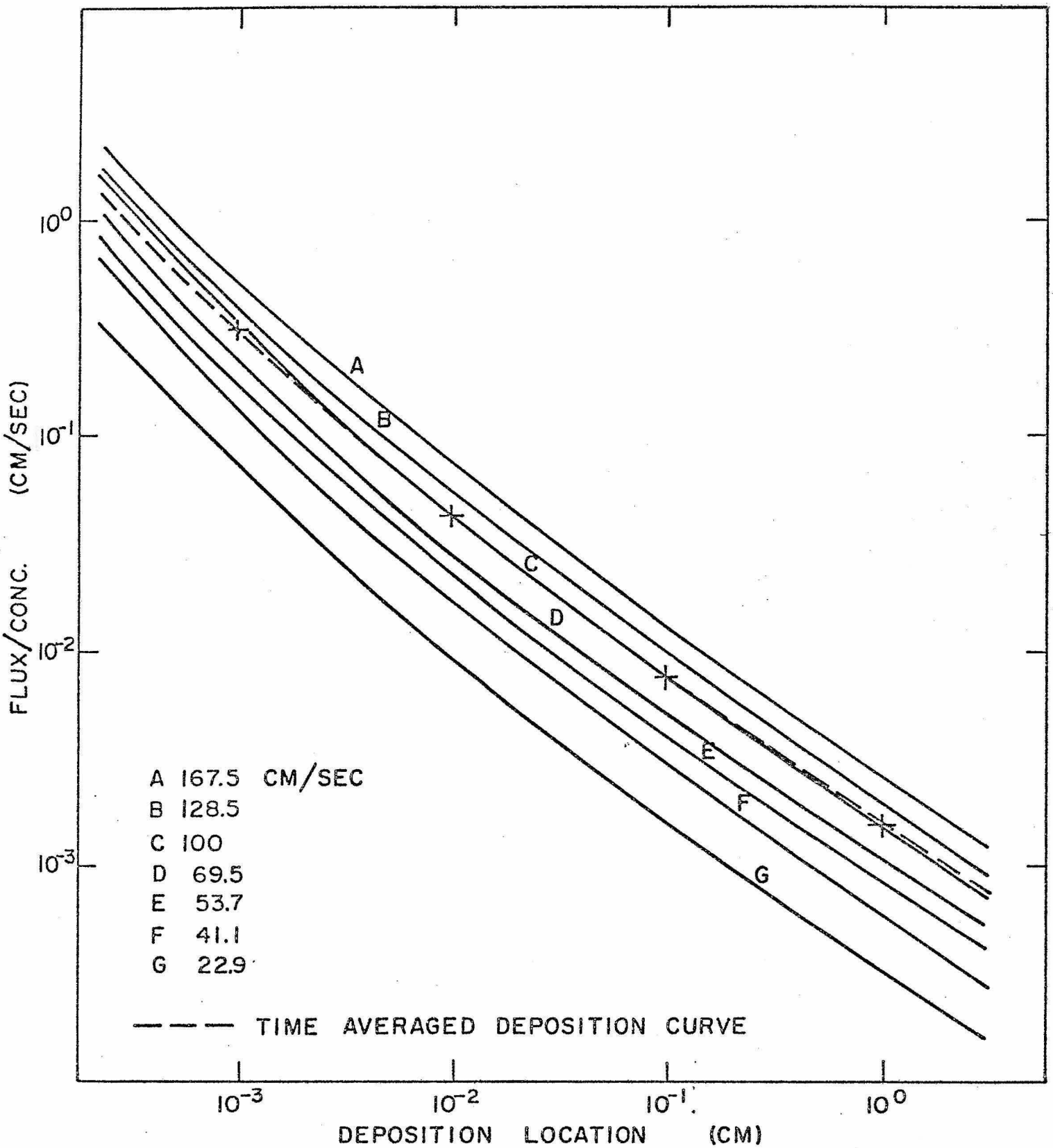

FIG. B2 1-MICRON PARTICLE DEPOSITION FOR VARIOUS POTENTIAL VELOCITIES AND THE TIME AVERAGED DEPOSITION CURVE FOR A 1 SEC. 300 GG INHALATION

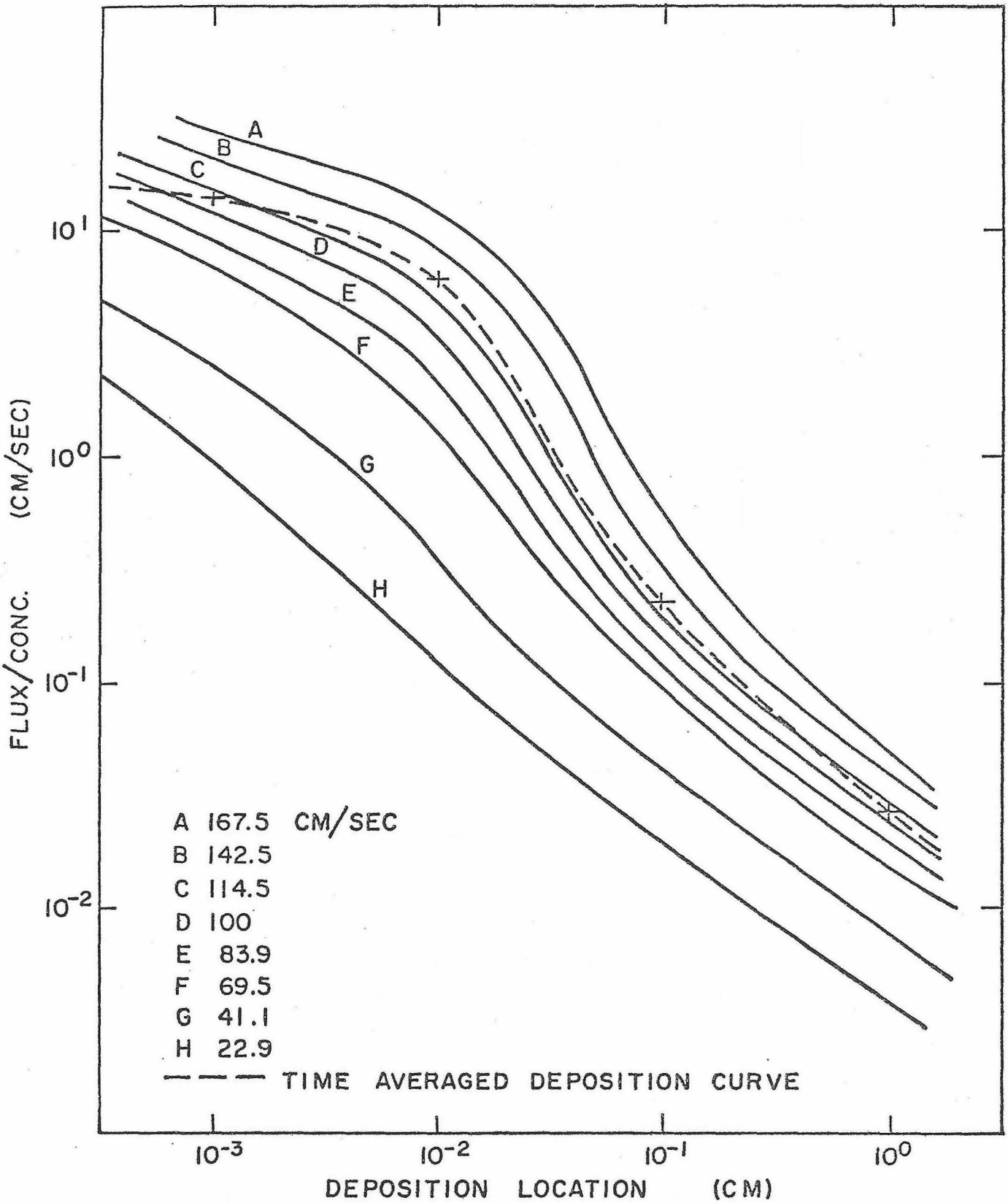

FIG. B3 10-MICRON PARTICLE DEPOSITION FOR VARIOUS POTENTIAL VELOCITIES AND THE TIME AVERAGED DEPOSITION CURVE FOR A 1 SEC 300 CC INHALATION

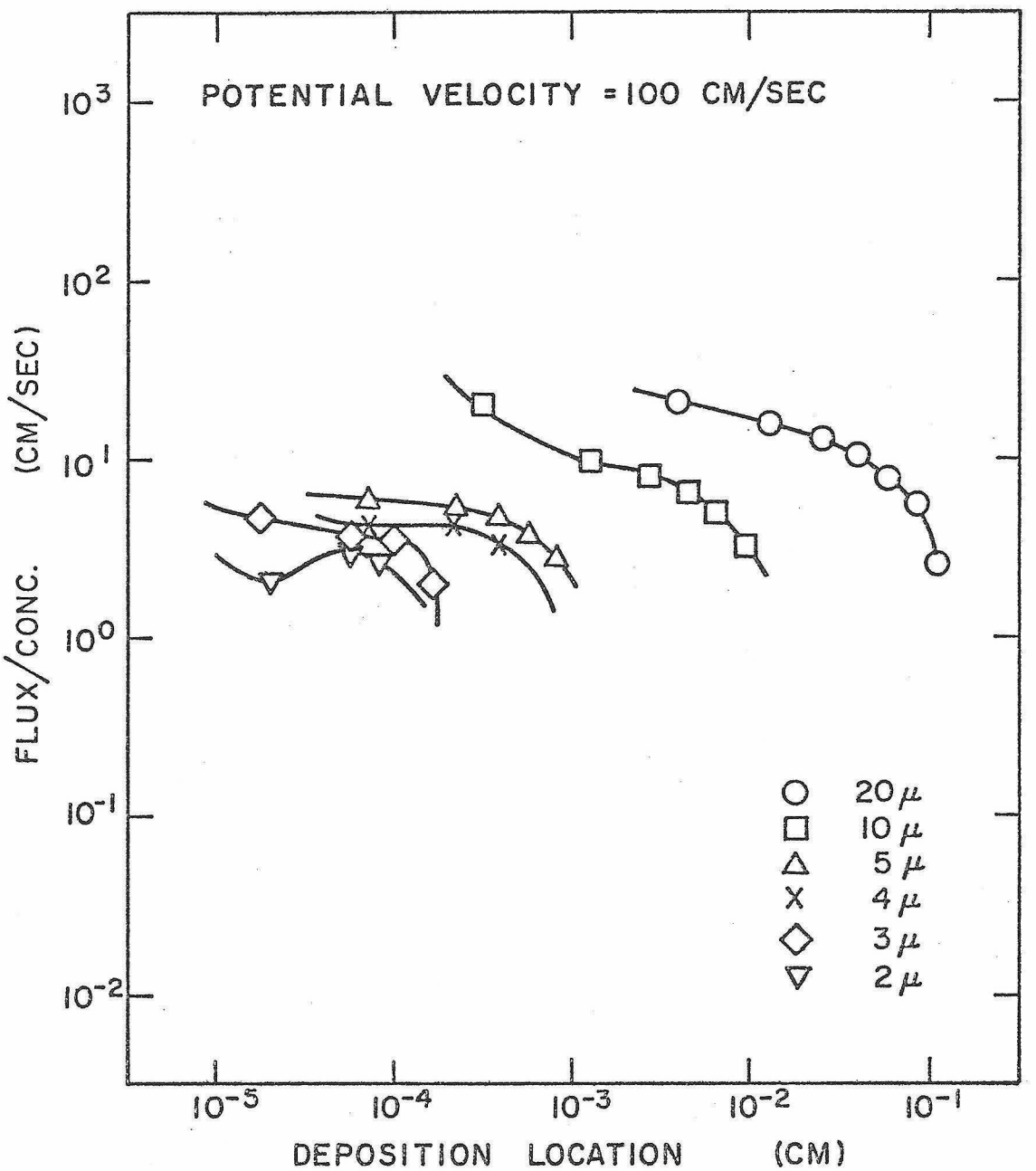

FIG. B4 STEADY LAMINAR BOUNDARY LAYER DEPOSITION CURVES FOR VARIOUS PARTICLE SIZES

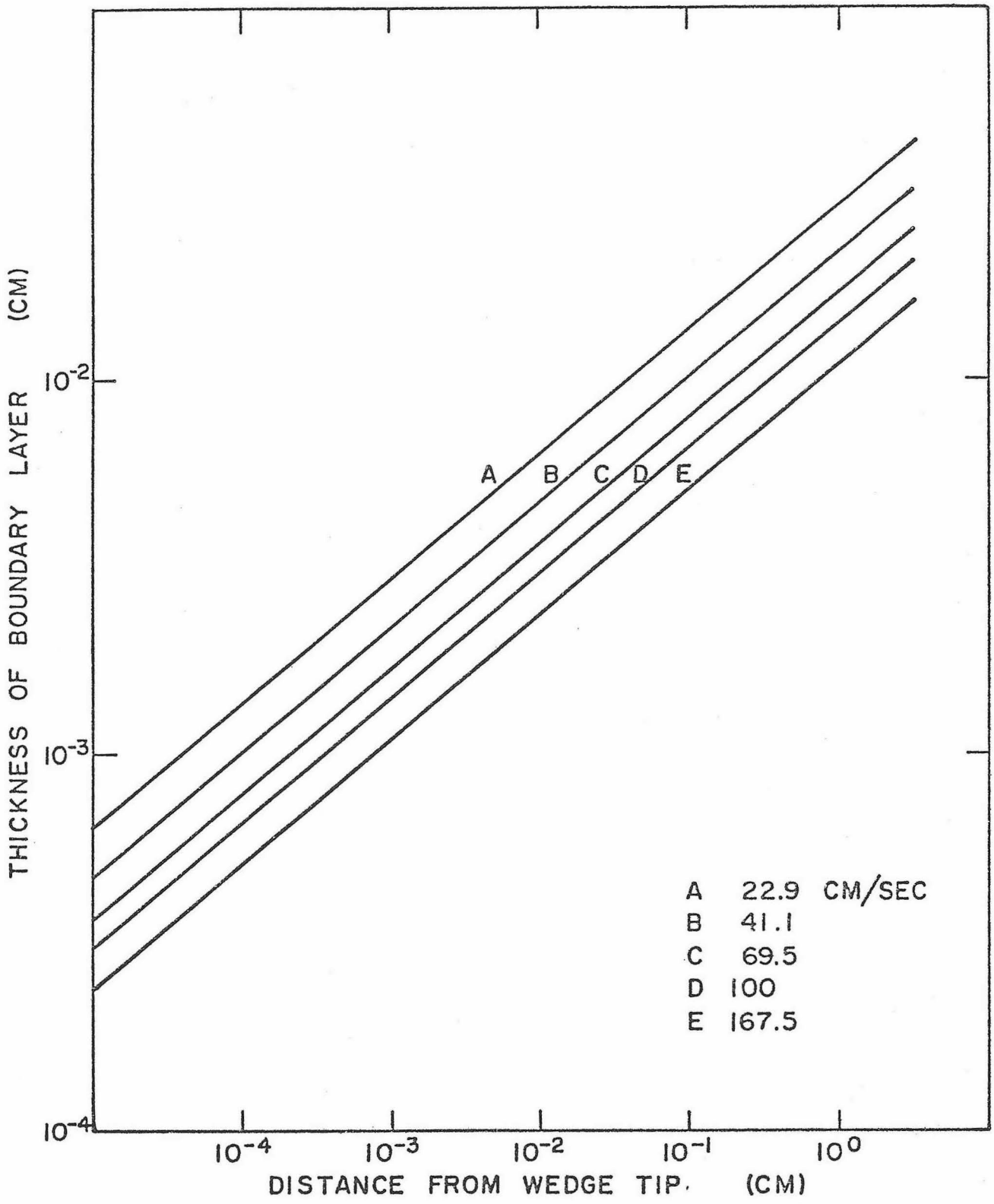

FIG. B5 STEADY LAMINAR BOUNDARY LAYER THICKNESS ALONG A 90° WEDGE FOR VARIOUS POTENTIAL VELOCITIES

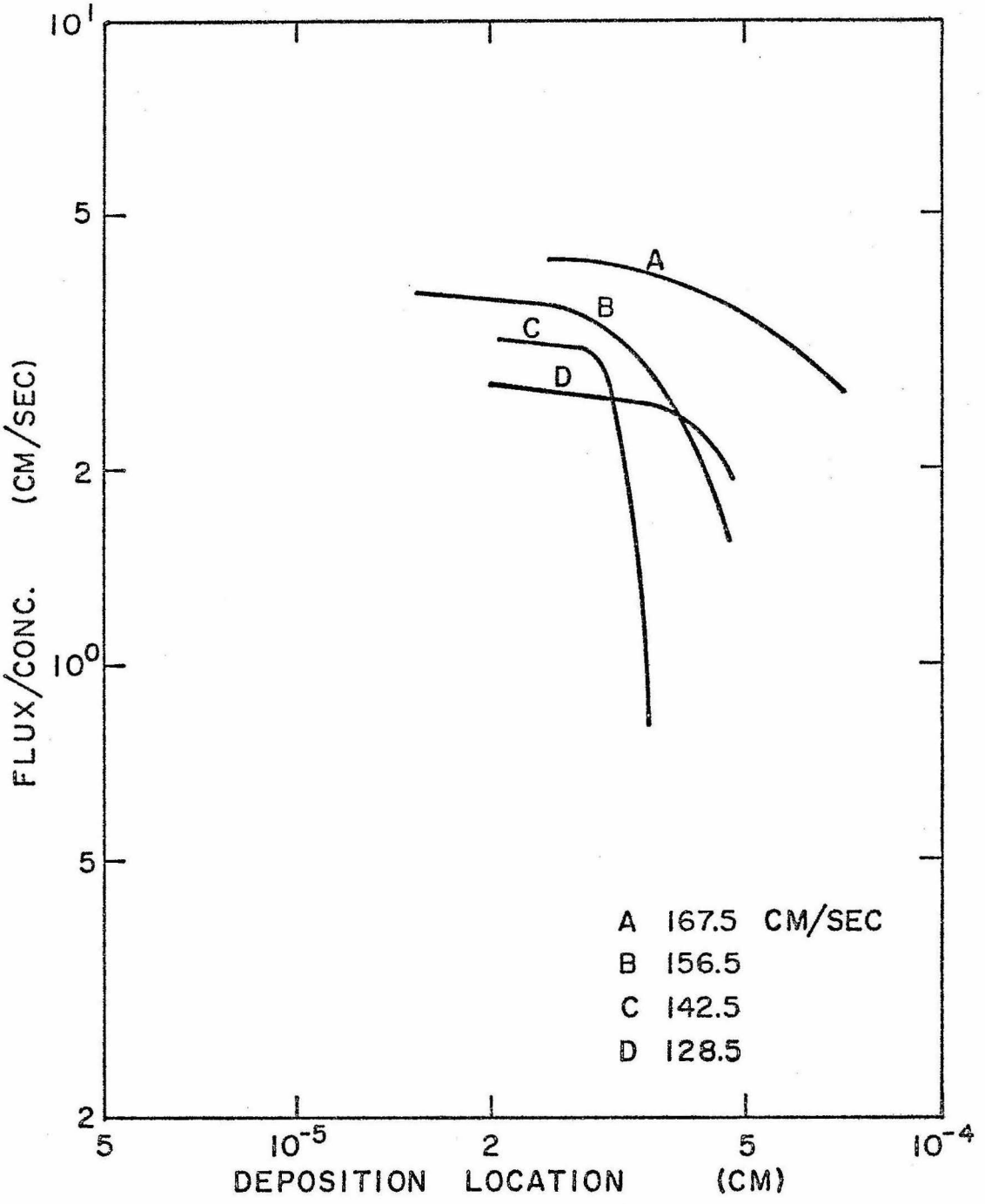

FIG. B6 ONE-MICRON PARTICLE DEPOSITION FOR VARIOUS POTENTIAL VELOCITIES WITH A STEADY LAMINAR BOUNDARY LAYER

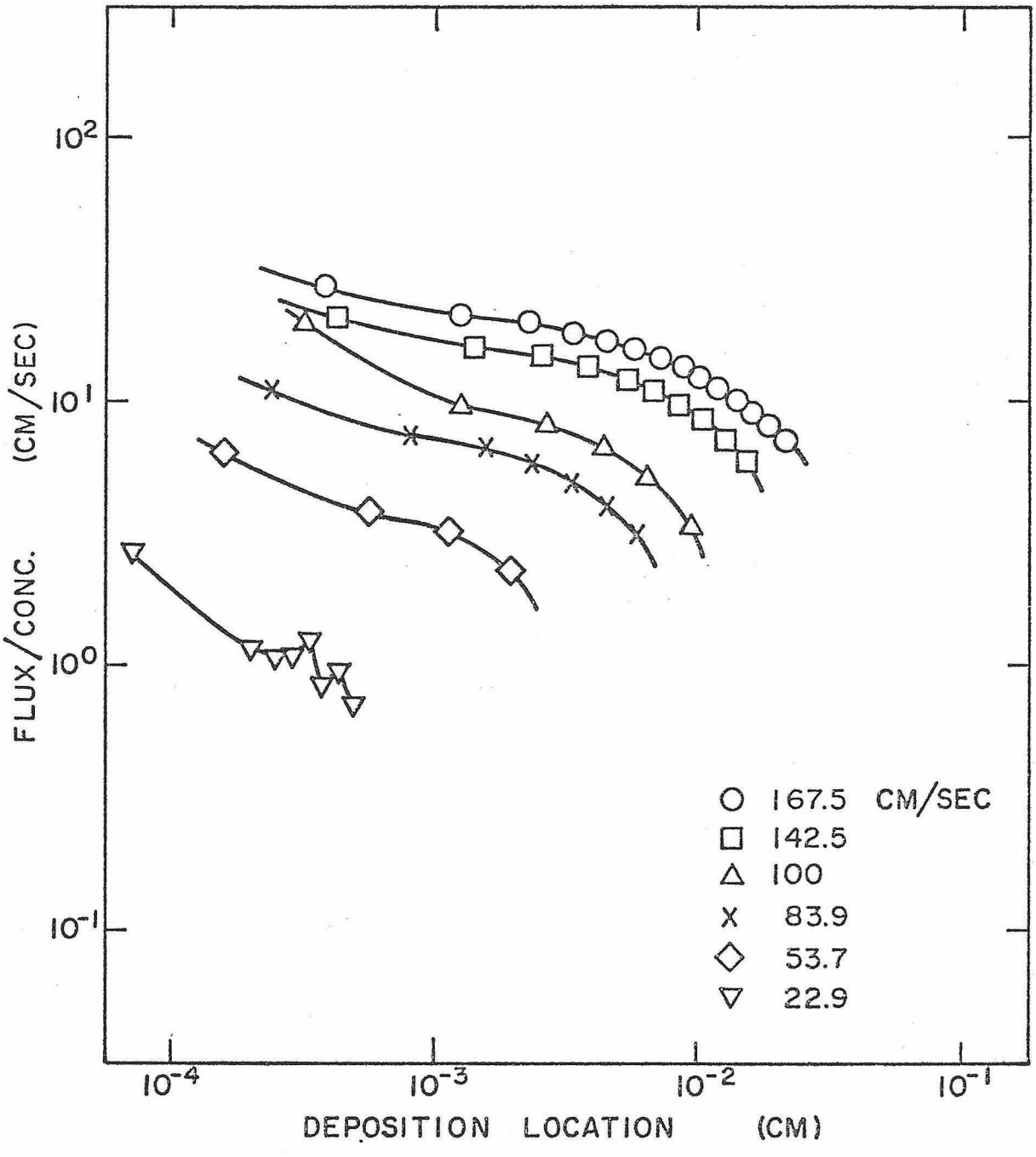

FIG. B7 10-MICRON PARTICLE DEPOSITION FOR VARIOUS POTENTIAL VELOCITIES WITH A STEADY LAMINAR BOUNDARY LAYER

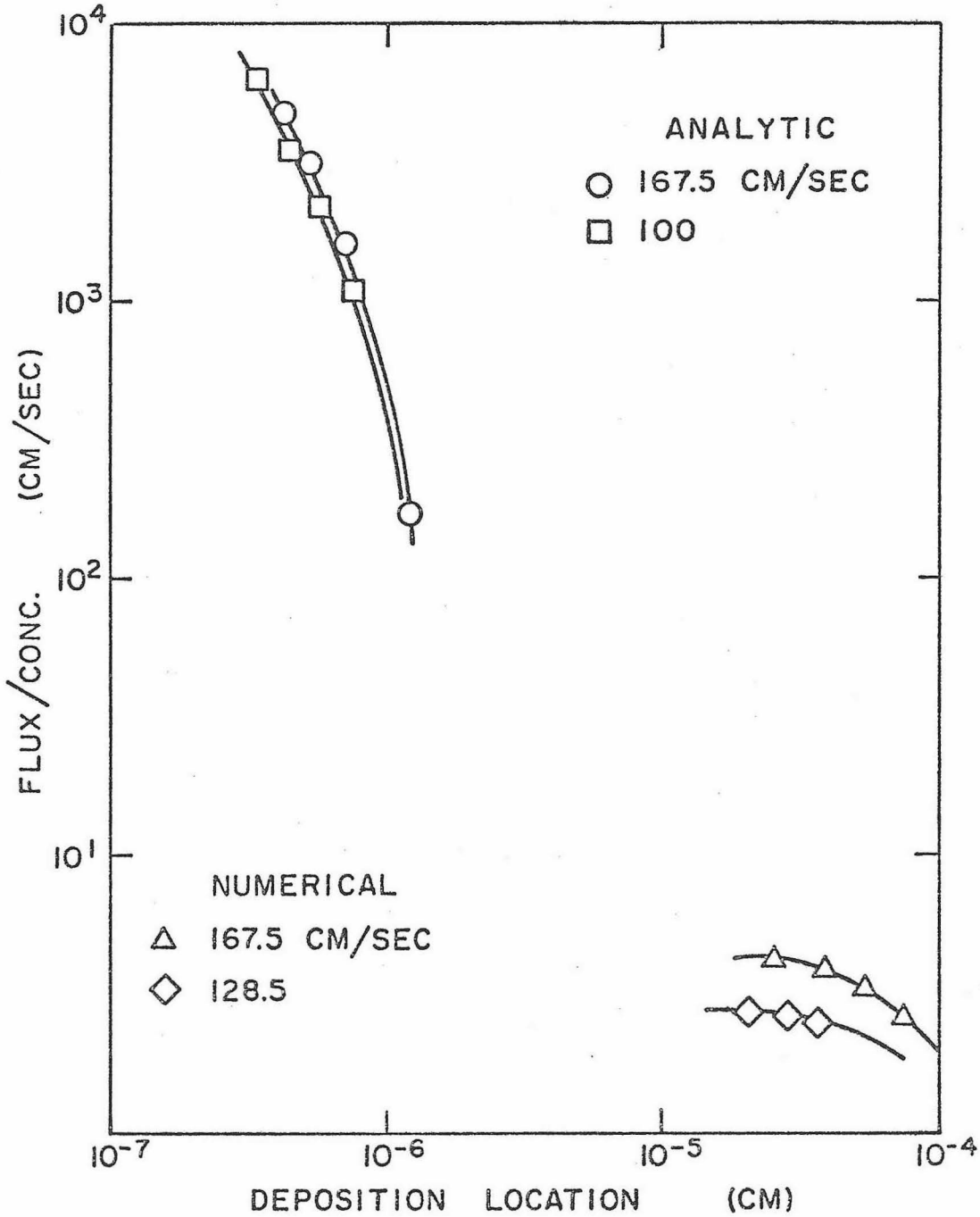

FIG. B8 NUMERIC AND ANALYTIC STEADY LAMINAR BOUNDARY LAYER SOLUTIONS FOR 1-MICRON PARTICLES

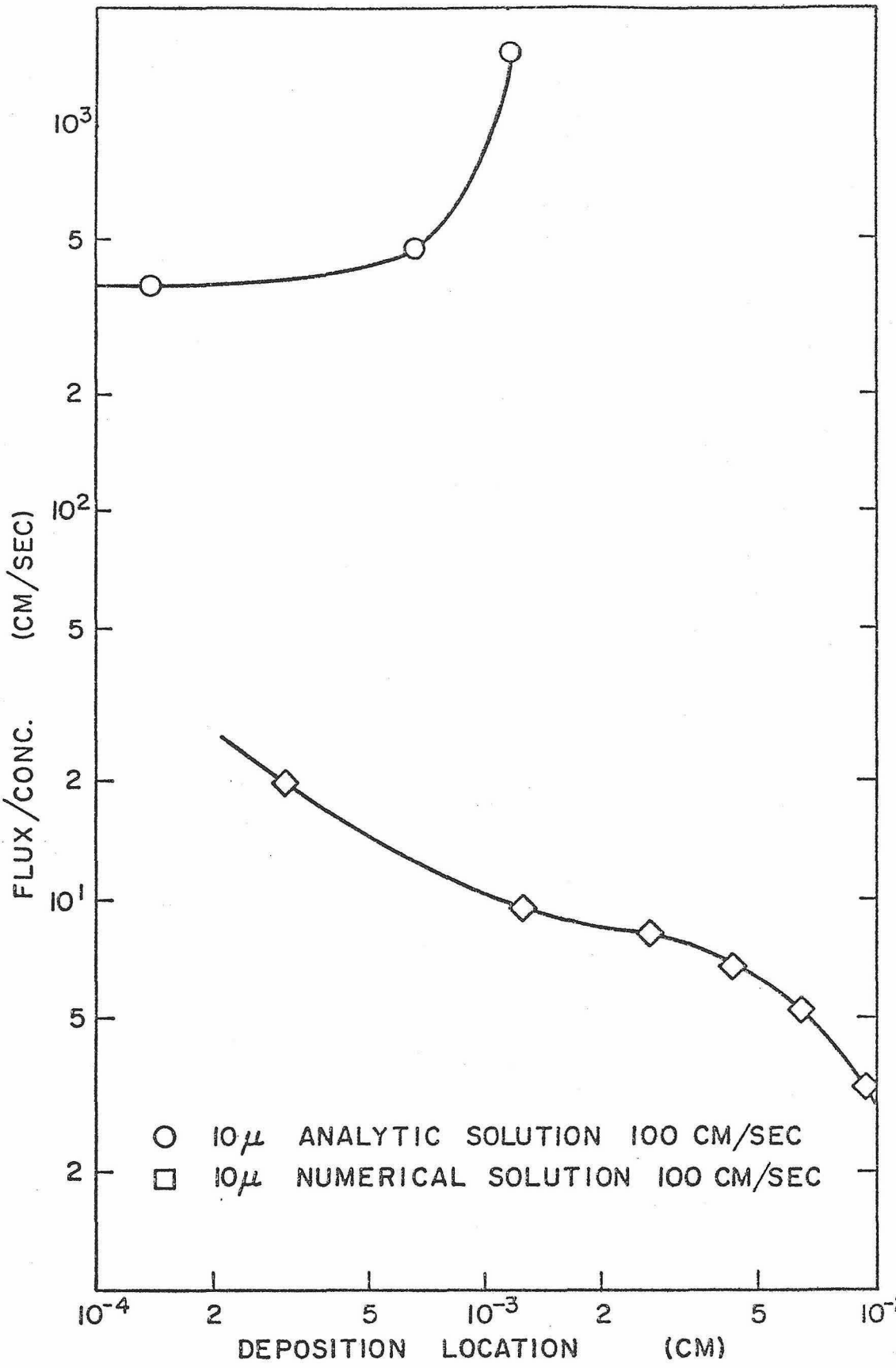

FIG. B9 NUMERIC AND ANALYTIC STEADY LAMINAR BOUNDARY LAYER SOLUTION FOR 10-MICRON PARTICLES

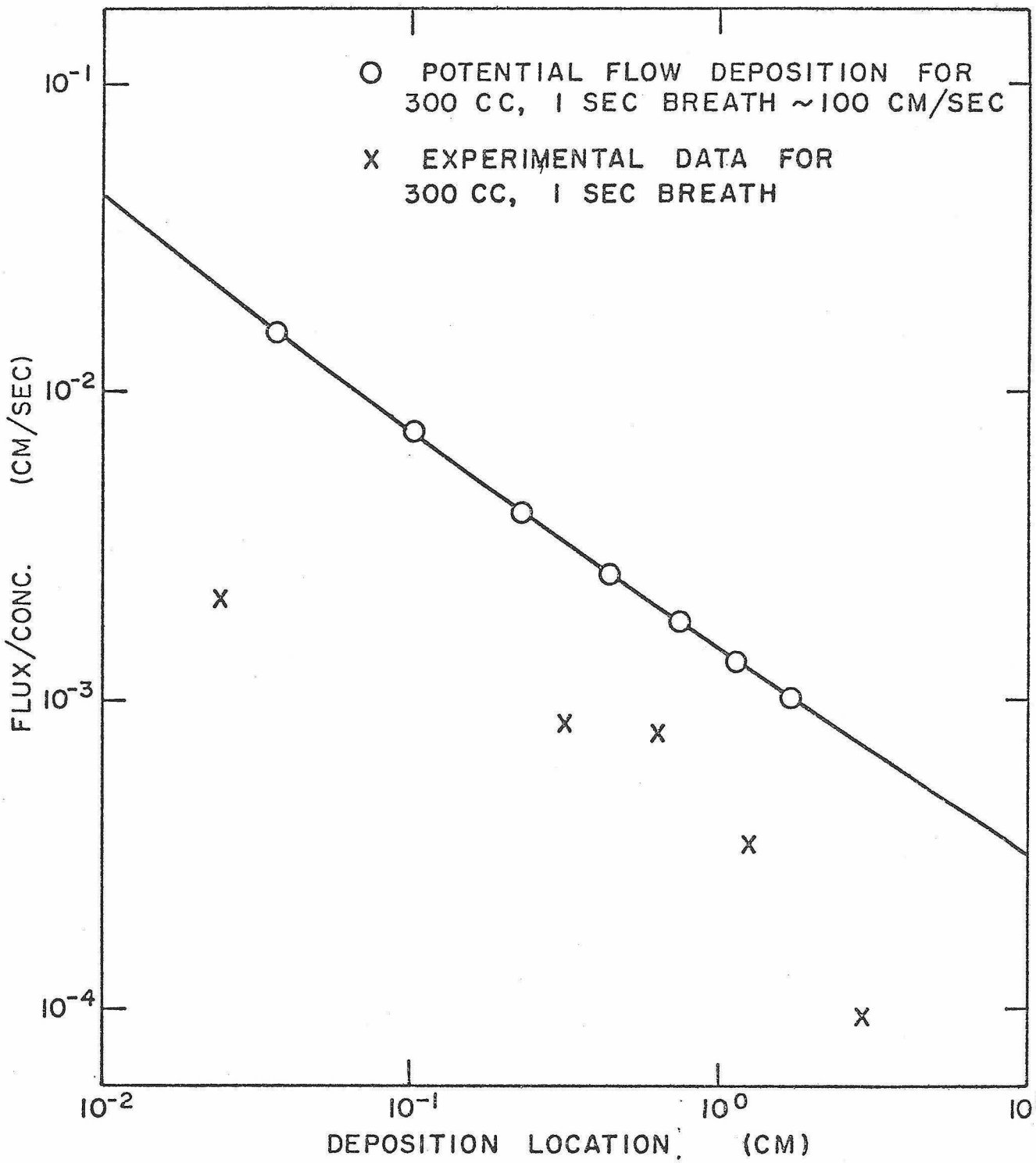

FIG. B10 COMPARISON OF THE INERTIAL POTENTIAL FLOW DEPOSITION THEORY WITH EXPERIMENTAL DATA FOR 1 MICRON PARTICLES IN A 1 SEC 300 CC INHALATION

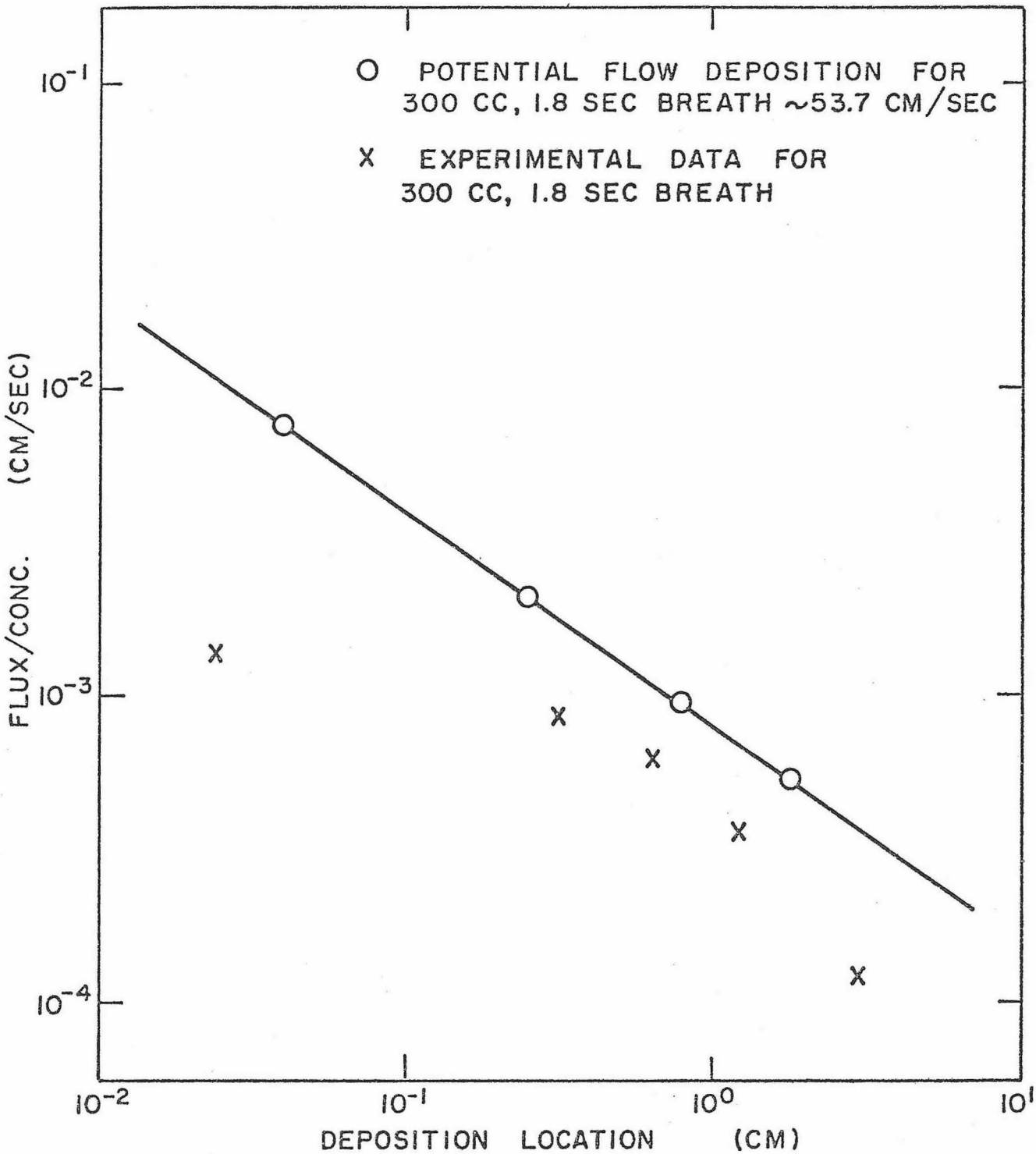

FIG. B11 COMPARISON OF THE INERTIAL POTENTIAL FLOW DEPOSITION THEORY WITH EXPERIMENTAL DATA FOR 1 MICRON PARTICLES IN A 1.8 SEC 300 CC INHALATION

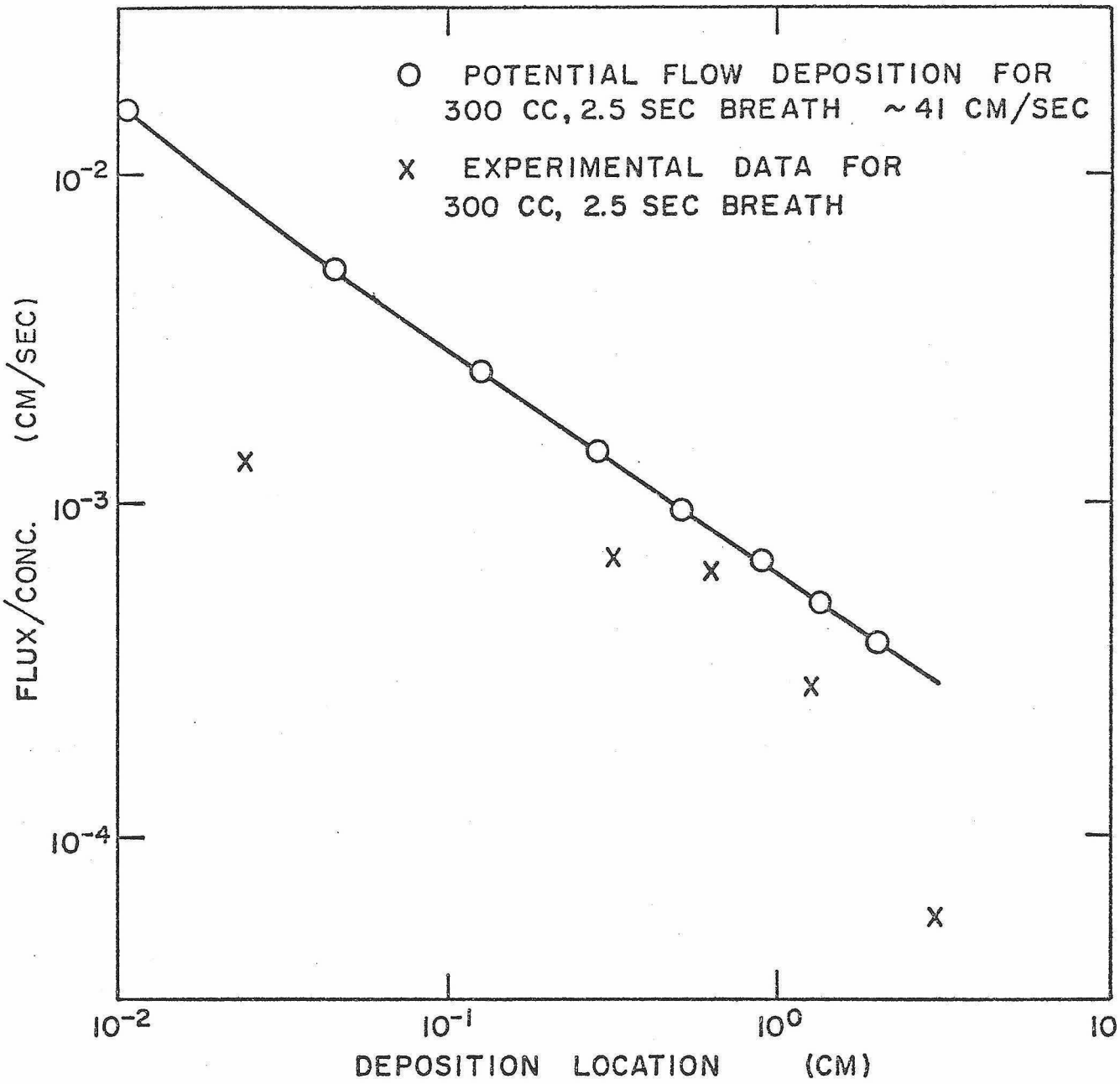

FIG. B12 COMPARISON OF THE INERTIAL POTENTIAL FLOW DEPOSITION THEORY WITH EXPERIMENTAL DATA FOR 1 MICRON PARTICLES IN A 2.5 SEC 300 CC INHALATION

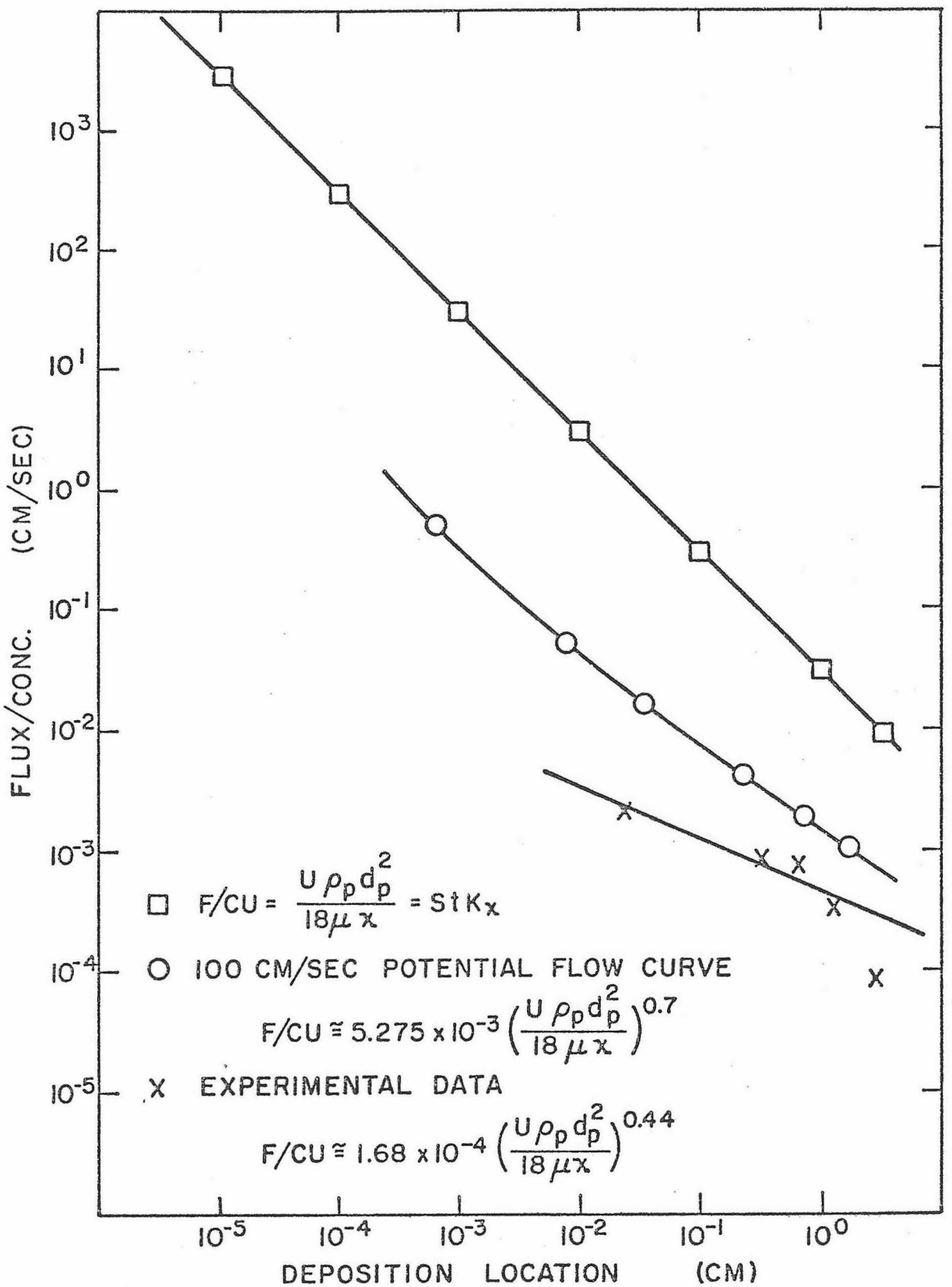

FIG. B13 STOKES DIMENSIONLESS CORRELATION FOR 1-MICRON PARTICLES

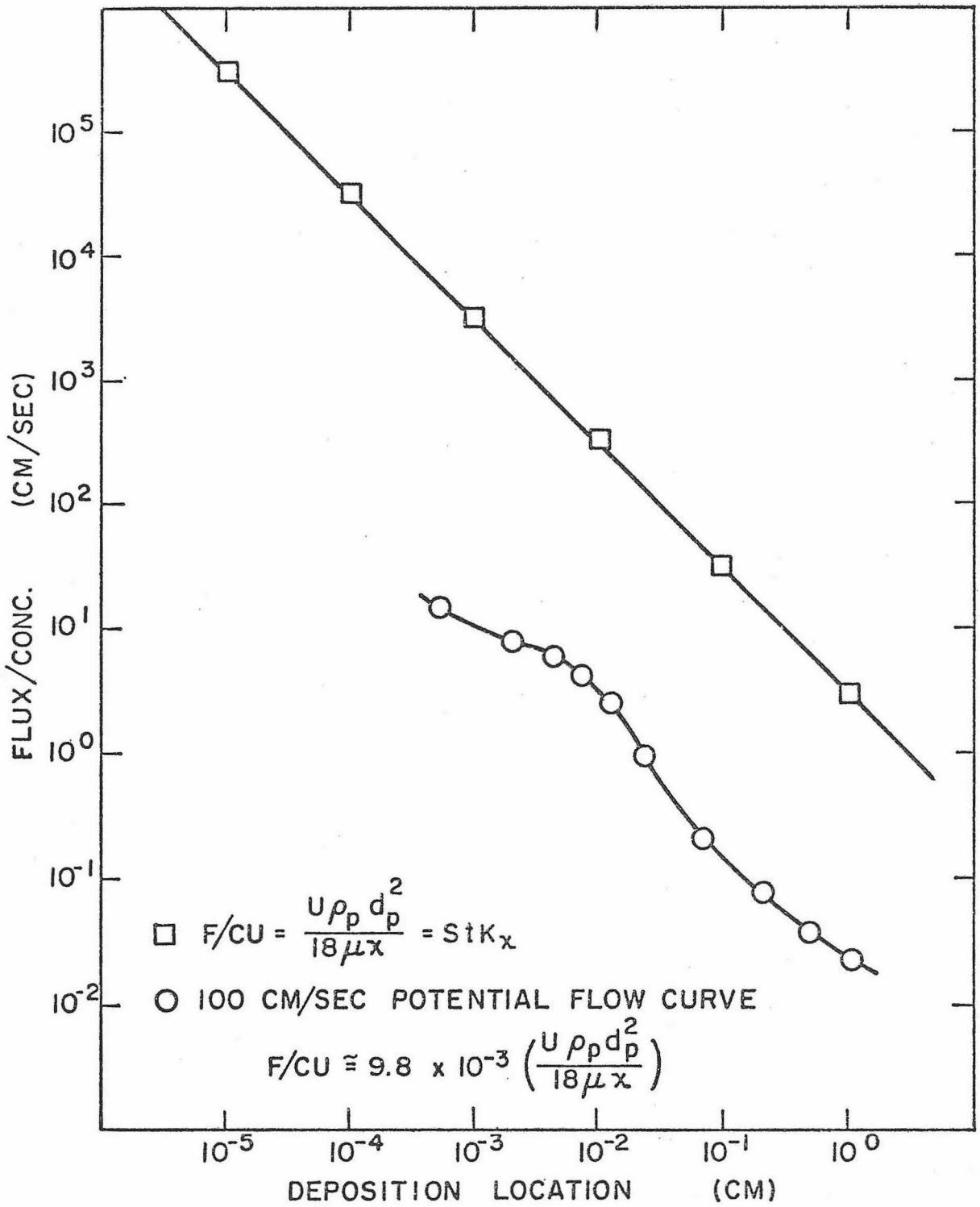

FIG. B14 STOKES DIMENSIONLESS CORRELATION FOR 10-MICRON PARTICLES

FIG. C1

MODEL TEST SECTION

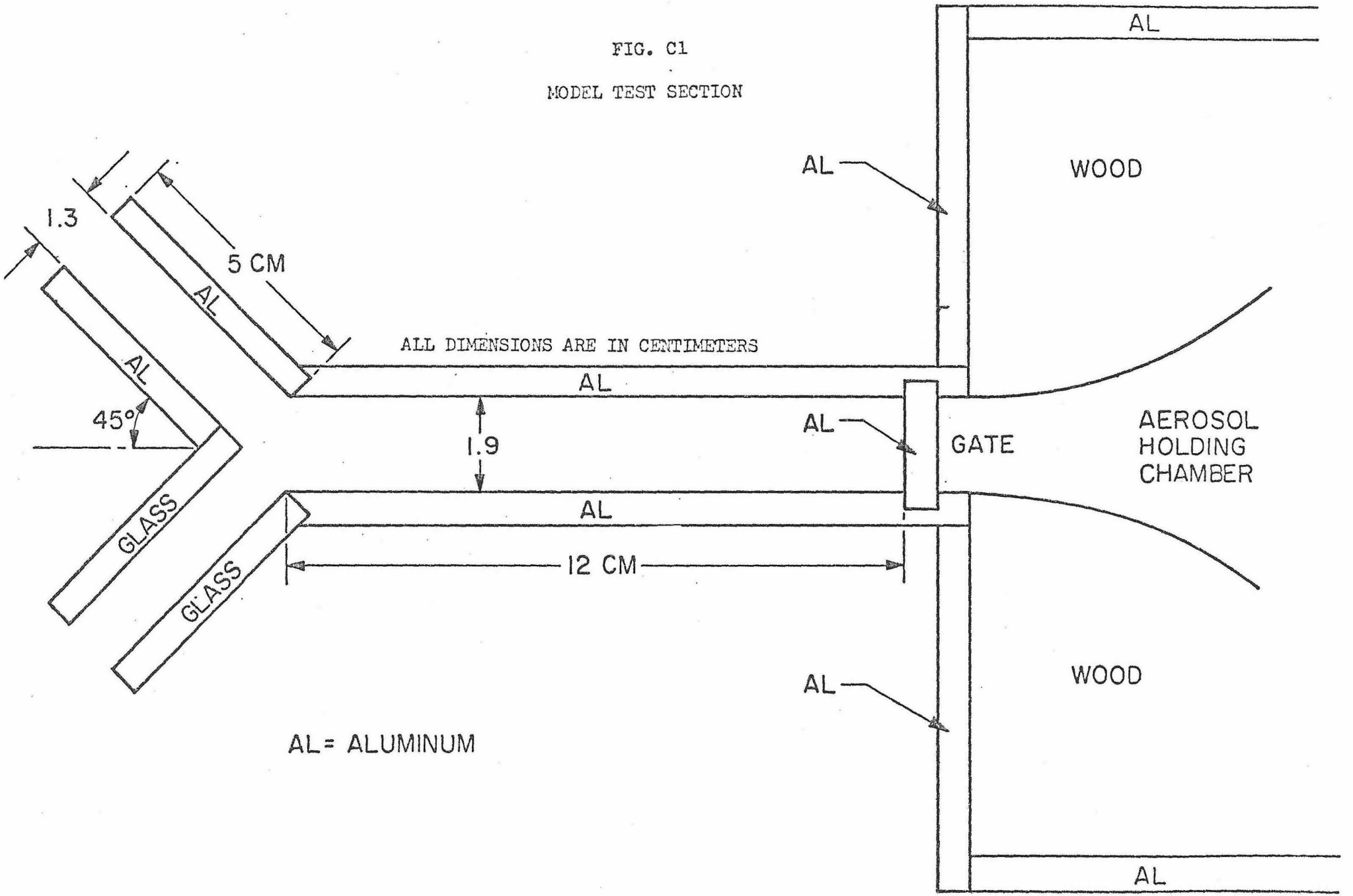

FIG. C2

SCHEMATIC OF EXPERIMENTAL LUNG APPARATUS

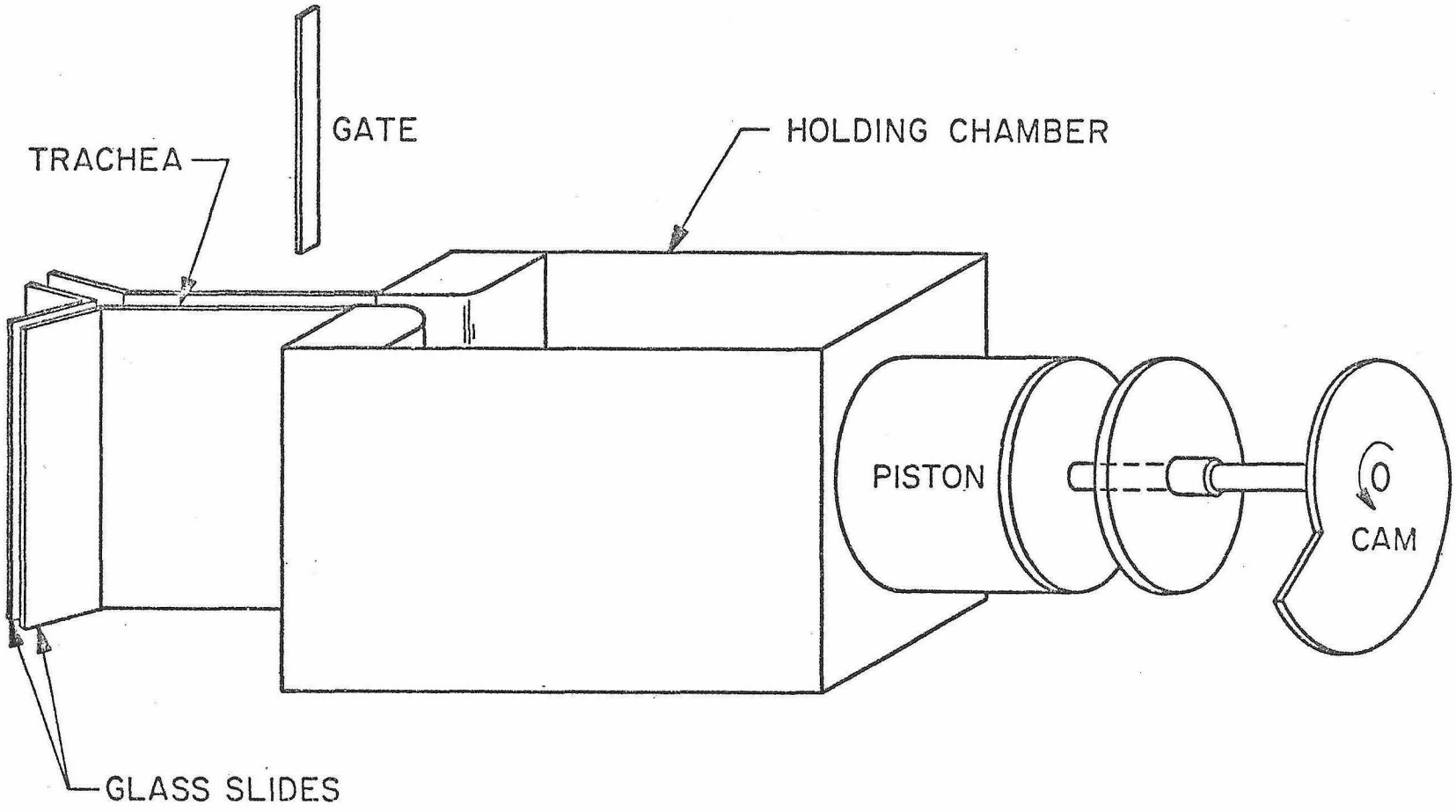

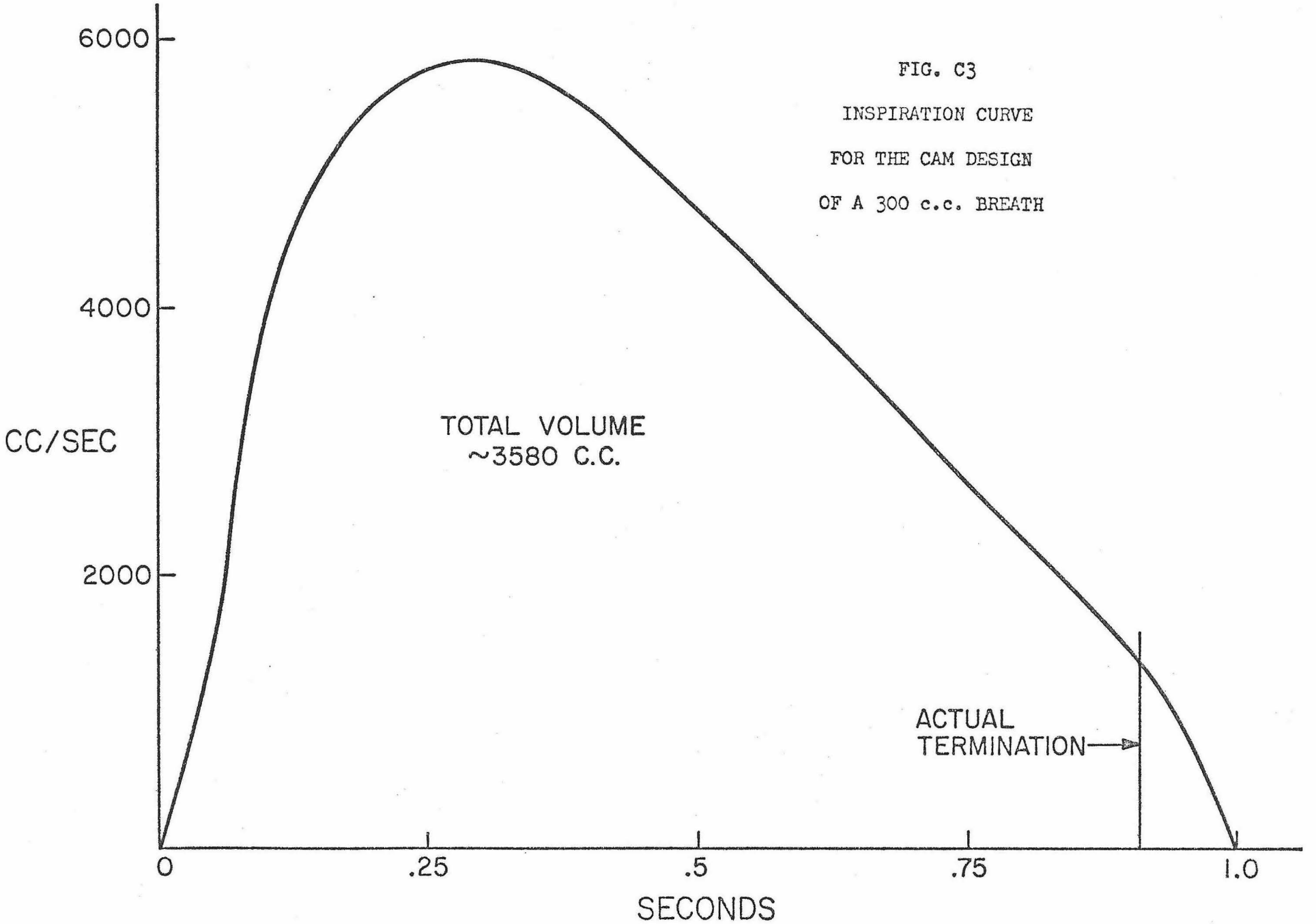

FIG. C3

INSPIRATION CURVE

FOR THE CAM DESIGN

OF A 300 c.c. BREATH

TABLE C1

Average flow rates and velocities calculated from cam curve of Figure C3

Time Segment Number	Time Segment Width-sec	Average Flow Rate cc/sec	Average Velocity cm/sec
1	1/16	787	22.9
2	1/16	3537	102.5
3	1/16	4912	142.5
4	1/16	5512	160.5
5	1/16	5762	167.5
6	1/16	5662	164.5
7	1/16	5381	156.5
8	1/16	4912	142.5
9	1/16	4412	128.5
10	1/16	3943	114.5
11	1/16	3412	99.0
12	1/16	2882	83.9
13	1/16	2381	69.5
14	1/16	1849	53.7
15	1/32	1412	41.1

```
C STEADY POTENTIAL FLOW PROGRAM TO CALCULATE THE AEROSOL DEPOSITION
C RATES AND LOCATIONS ALONG THE WEDGE IN A BIFURCATION LUNG MODEL
C
C
C DEFINITION OF VARIABLES
C
C      XO,YO= PARTICLE COORDINATES AT STARTING POSITION
C      X1,Y1,X2,Y2= PARTICLE COORDINATES AT  EGINNING AND END OF EACH
C      TRAJECTORY SEGMENT
C      UX,UY= PARTICLE AND STREAM VELOCITY COMPONENTS AT STARTING POSITION
C      UX1,UY1= STREAM VELOCITY COMPONENT AT BEGINNING OF EACH SEGMENT
C      VX1,VY1,VX2,VY2= PARTICLE VELOCITY COMPONENT AT BEGINNING AND END
C      OF EACH SEGMENT
C      LIM= MAXIMUM NUMBER OF STARTING POSITIONS
C      DELZ= VERTICAL DISTANCE BETWEEN STARTING POSITIONS
C      TAU= PARTICLE RELAXATION TIME
C      R= PARTICLE RADIUS
C      C=MAXIMUM DISTANCE OF TRAVEL ALLOWABLE ALONG WEDGE
C      DT= TIME INTERVAL FOR EACH SEGMENT
C      U= STREAM VELOCITY AT INFINITY
C      U1= STREAM VELOCITY AT
C      STAGNATION STREAMLINE
C      U1= STREAM VELOCITY AT ONE CENTIMETER BEFORE THE WEDGE ON THE
C      XL= PARTICLE DEPOSITION LOCATION ALONG WEDGE FOR ONE RUN
C      ZL= AVERAGE DEPOSITION LOCATION FOR TWO XL LOCATIONS
C      FSC= DEPOSITION FLUX/PARTICLE CONCENTRATION IN STREAM
C
C MAIN PROGRAM TO DETERMINE PARTICLE TRAJECTORIES
      COMMON UX(40),UY(40),XL(40),DELZ,N
     ODOUBLE PRECISION DELZ,XO,YO,THETA,DIST6,DIST,ZANGLE,VX1,VY1,X1,Y1,
     1UX1,UY1,RELX,T,X2,Y2,VX2,VY2,Z,XL,UX,UY,SLOEP,U1
      DIST6(A,B)=U1*(A*A+B*B)**.1666666666666666
    5 READ(5,10) LIM,DELZ,XO,TAU,R,C,DT,DT1
   10 FORMAT(I10,2D10.5,5E10.5)
      IF(LIM .LT. 1) STOP
      READ(5,11) U
   11 FORMAT(E10.5)
      U1=U/1.22
      WRITE(6,12) LIM,DELZ,XO,TAU,R,C,DT,U1
  120FORMAT(6HILIM =,I5,5X,6HDELZ =,D10.3,10X,4HXO =,D10.3,10X,5HTAU =,
     1E10.3//4H R =,E10.3,10X,3HC =,E10.3,10X,4HDT =,E10.3,10X,4HU1 =,E1
     20.3/////)
      DT2=DT
C
C     START OF MAIN DO LOOP FOR EACH NEW STARTING POSITION
C
      DO 69 I=1,LIM
      T=(-DT2)/TAU
      RELX=1.0-DEXP(T)
      RUN=FLOAT(I)
C
C     CALC OF INITIAL PARTICLE VELOCITIES
C
      YO=DELZ*(RUN-1.0)+.00000000000000001
      THETA=DATAN2(YO,XO)
      ZANGLE=(3.14159265358979 32-THETA)/3.0
      DIST=DIST6(XO,YO)
      UX(I)=DIST*DCOS(ZANGLE)
      UY(I)=DIST*DSIN(ZANGLE)
      WRITE(6,15)I,XO,YO,UX(I),UY(I)
  150FORMAT(12HORUN NUMBER=,I4,3X,3HXO=,D13.5,4X,3HYO=,D13.5,5X,7HUX(I)
```

```
     1 =,D13.5,5X,7HUY(I) =,D13.5//)
       VX1=UX(I)
       VY1=UY(I)
       X1=XO
       Y1=YO
       J=1
C
C      PARTICLE VELOCITIES AND POSITIONS CALC IN POTENTIAL FLOW REGIME
C
    20 THETA=DATAN2(Y1,X1)
       ZANGLE=(3.14159265358979 32-THETA)/3.0
       DIST=DIST6(X1,Y1)
       UX1=DIST*DCOS(ZANGLE)
       UY1=DIST*DSIN(ZANGLE)
       VX2=VX1+(UX1-VX1)*RELX
       VY2=VY1+(UY1-VY1)*RELX
       X2=X1+UX1*DT+TAU*(VX1-UX1)*RELX
       Y2=Y1+UY1*DT+TAU*(VY1-UY1)*RELX
       Z=DSQRT(X2*X2+Y2*Y2)
C
C     CHECK IF PARTICLES HAVE IMPACTED ON THE WEDGE WALL
C
       IF(X2 .LT. -.01) GO TO 23
       IF(Z .LE. R) GO TO 30
       IF(X2 .GE. 0.0 .AND. Y2 .LE. R) GO TO 30
       IF(Y2 .LE. (X2+1.414214*R)) GO TO 40
       IF(X2 .GE. 0.0 .AND. Z .GT. C) GO TO 50
    23 X1=X2
       Y1=Y2
       VX1=VX2
       VY1=VY2
       GO TO 20
C
C     CALCULATION OF EXACT DEPOSITION LOCATIONS
C
    30 XL(I)=0.0
       GO TO 69
    40 SLOEP=(Y2-Y1)/(X2-X1)
       XL(I)=1.414214*(((Y1-SLOEP*X1-1.414214*R)/(1-SLOEP))+.70711*R)
       IF(XL(I) .LT. 0.0) XL(I)=0.0
    69 CONTINUE
       N=IFIX(RUN-.9)
       M=N
       GO TO 54
    50 N=IFIX(RUN-1.9)
       M=N+1
    54 WRITE(6,51)
    51 FORMAT(1H1,15X,2HUX,18X,2HUY,18X,2HXL//)
       WRITE(6,52) (UX(I),UY(I),XL(I), I=1,M)
    52 FORMAT(1H0,3D20.8)
       WRITE(6,53)
    53 FORMAT(1H1)
       CALL DEPOST
       GO TO 5
       END
C SUBROUTINE TO CALCULATE THE DEPOSITION RATES AND LOCATIONS
       SUBROUTINE DEPOST
       COMMON UX(40),UY(40),XL(40),DELZ,N
       DOUBLE PRECISION AVUX,AVUY,AVEL,ANGL,ZL,FSC,DELZ,UX,UY,XL
       WRITE(6,5)
     5 FORMAT(1H0,20X,17HAVER DEP LOCATION,26X,13HDEP FLUX/CONC//)
```

```
      DO 15 K=1,N
      AVUX=(UX(K)+UX(K+1))/2.0
      AVUY=(UY(K)+UY(K+1))/2.0
      AVEL=DSQRT(AVUX*AVUX+AVUY*AVUY)
      ANGL=DATAN2(AVUY,AVUX)
      ZL=(XL(K)+XL(K+1))/2.0
      IF(ZL .LE. 0.0) GO TO 7
      FSC=AVEL*DELZ*DCOS(ANGL)/(XL(K+1)-XL(K))
      GO TO 9
    7 FSC=AVEL*DELZ*DCOS(ANGL)/(.0000I)
    9 WRITE(6,25) ZL,FSC
   25 FORMAT(1H0,20X,D20.8,20X,D20.8)
   15 CONTINUE
      RETURN
      END
```

```
C  STEADY POTENTIAL FLOW WITH LAMINAR BOUNDARY LAYER PROGRAM TO CALCULATE
C       THE AEROSOL DEPOSITION RATES AND LOCATIONS ALONG THE WEDGE IN A
C       BIFURCATION LUNG MODEL
C
C  DEFINITION OF VARIABLES
C
C       XO,YO= PARTICLE COORDINATES AT STARTING POSITION
C       X1,Y1,X2,Y2= PARTICLE COORDINATES AT BEGINNING AND END OF EACH
C       TRAJECTORY SEGMENT
C       UX,UY= PARTICLE AND STREAM VELOCITY COMPONENTS AT STARTING POSITION
C       UX1,UY1= STREAM VELOCITY COMPONENT AT BEGINNING OF EACH SEGMENT
C       VX1,VY1,VX2,VY2= PARTICLE VELOCITY COMPONENT AT BEGINNING AND END
C       OF EACH SEGMENT
C       LIM= MAXIMUM NUMBER OF STARTING POSITIONS
C       DELZ= VERTICAL DISTANCE BETWEEN STARTING POSITIONS
C       TAU= PARTICLE RELAXATION TIME
C       R= PARTICLE RADIUS
C       C=MAXIMUM DISTANCE OF TRAVEL ALLOWABLE ALONG WEDGE
C       DT= TIME INTERVAL FOR EACH SEGMENT
C       DT1= TIME INTERVAL FOR A TRAJECTORY SEGMENT IN THE BOUNDARY LAYER
C       U= STREAM VELOCITY AT INFINITY
C       U1= STREAM VELOCITY AT INFINITY
C       STAGNATION STREAMLINE
C       U1= STREAM VELOCITY AT ONE CENTIMETER BEFORE THE WEDGE ON THE
C       XL= PARTICLE DEPOSITION LOCATION ALONG WEDGE FOR ONE RUN
C       ZL= AVERAGE DEPOSITION LOCATION FOR TWO XL LOCATIONS
C       FSC= DEPOSITION FLUX/PARTICLE CONCENTRATION IN STREAM
C       XMUP= MOMENTUM DIFFUSIVITY OF AIR
C       BLT= BOUNDARY LAYER THICKNESS AT XB
C       XB= COORDINATE ALONG WEDGE
C       YB= COORDINATE PERPENDICULAR TO WEDGE
C       UXB,UYB,= BOUNDARY LAYER VELOCITIES IN XB,YB DIRECTIONS
C
C  MAIN PROGRAM TO DETERMINE PARTICLE TRAJECTORIES
      COMMON UX(40),UY(40),XL(40),DELZ,N
     0DOUBLE PRECISION DELZ,XO,YO,THETA,DIST6,DIST,ZANGLE,VX1,VY1,X1,Y1,
     1UX1,UY1,RELX,T,X2,Y2,VX2,VY2,Z,XL,UX,UY,SLOEP,F1,F12,F13,F32,F52,F
     230,G,BCF,ZINGLE,YB,XB,BLT,XB13,XB43,XB73,YB20,YB30,YB50,YB60,UXB,U
     3YB
      DIST6(A,B)=U1*(A*A+B*B)**.1666666666666666
    5 READ(5,10) LIM,DELZ,XO,TAU,R,C,DT,DT1
   10 FORMAT(I10,2D10.5,5E10.5)
      IF(LIM .LT. 1) STOP
      READ(5,11) U
   11 FORMAT(E10.5)
      U1=U/1.22
      WRITE(6,12) LIM,DELZ,XO,TAU,R,C,DT,DT1,U1
  120FORMAT(6H1LIM =,I5,5X,6HDELZ =,D10.3,10X,4HXO =,D10.3,10X,5HTAU =,
     1E10.3//4H R =,E10.3,10X,3HC =,E10.3,10X,4HDT =,E10.3,10X,6HDT1 = ,
     2E10.3,10X,4HU1 =,E10.3/////)
      DT2=DT
      XMUP= 0.166
      F=U1/XMUP
      F12=F**.5
      F13=F**.3333333333333333
      F32=F**1.5
      F52=F**2.5
      F30=F**3.0
      G=(U1*XMUP)**.5
      BCF=3.43/F12
C
```

```
C       START OF MAIN DO LOOP FOR EACH NEW STARTING POSITION
C
        DO 69 I=1,LIM
        T=(-DT2)/TAU
        RELX=1.0-DEXP(T)
        RUN=FLOAT(I)
C
C     CALC OF INITIAL PARTICLE VELOCITIES
C
        YO=DELZ*(RUN-1.0)+.00000000000000001
        THETA=DATAN2(YO,XO)
        ZANGLE=(3.14159265358979 32-THETA)/3.0
        DIST=DIST6(XO,YO)
        UX(I)=DIST*DCOS(ZANGLE)
        UY(I)=DIST*DSIN(ZANGLE)
        WRITE(6,15)I,XO,YO,UX(I),UY(I)
   150FORMAT(12HORUN NUMBER=,I4,3X,3HXO=,D13.5,4X,3HYO=,D13.5,5X,7HUX(I)
     1 =,D13.5,5X,7HUY(I) =,D13.5//)
        VX1=UX(I)
        VY1=UY(I)
        X1=XO
        Y1=YO
        J=1
C
C       PARTICLE VELOCITIES AND POSITIONS CALC IN POTENTIAL FLOW REGIME
C
    20  THETA=DATAN2(Y1,X1)
        ZANGLE=(3.14159265358979 32-THETA)/3.0
        DIST=DIST6(X1,Y1)
        UX1=DIST*DCOS(ZANGLE)
        UY1=DIST*DSIN(ZANGLE)
        VX2=VX1+(UX1-VX1)*RELX
        VY2=VY1+(UY1-VY1)*RELX
        X2=X1+UX1*DT+TAU*(VX1-UX1)*RELX
        Y2=Y1+UY1*DT+TAU*(VY1-UY1)*RELX
        Z=DSQRT(X2*X2+Y2*Y2)
C
C     CHECK IF PARTICLES HAVE IMPACTED ON THE WEDGE WALL
C
        IF(X2 .LT. -.01) GO TO 23
        IF(Z .LE. R) GO TO 30
        IF(X2 .GE. 0.0 .AND. Y2 .LE. R) GO TO 30
        IF(Y2 .LE. (X2+1.414214*R)) GO TO 40
        IF(X2 .GE. 0.0 .AND. Z .GT. C) GO TO 50
        THETA=DATAN2(Y2,X2)
        ZINGLE=THETA-(3.14159265358979 32/4.)
        YB=Z*DSIN(ZINGLE)
        XB=Z*DCOS(ZINGLE)
        IF(XB .LT. 0.0) GO TO 23
C     CALC OF BOUNDARY LAYER THICKNESS
        BLT=BCF*XB**.3333333333333333
        IF(YB .LE. BLT) GO TO 80
    23  X1=X2
        Y1=Y2
        VX1=VX2
        VY1=VY2
        GO TO 20
    80  VX1=VX2
        VY1=VY2
        X1=X2
        Y1=Y2
```

```
C
C       PARTICLE VELOCITIES AND POSITIONS CALC IN BOUNDARY LAYER
C
   81 THETA=DATAN2(Y1,X1)
      ZINGLE=THETA-(3.14159265358979327/4.)
      YB=Z*DSIN(ZINGLE)
      XB=Z*DCOS(ZINGLE)
      XB13=1.0/XB**.3333333333333333
      XB43=1.0/XB**1.3333333333333333
      XB73=1.0/XB**2.3333333333333333
      YB20=YB*YB
      YB30=YB20*YB
      YB50=YB30*YB20
      YB60=YB30*YB30
      UXB=U1*(.8*F12*YB-.166*F*YB20*XB13+.00148*F52*YB50*XB43)
      UYB=G*(-.018*F32*YB30*XB43+.000328*F30*YB60*XB73)
      UX1=.70711*(UXB-UYB)
      UY1=.70711*(UXB+UYB)
      VX2=VX1+(UX1-VX1)*RELX
      VY2=VY1+(UY1-VY1)*RELX
      X2=X1+UX1*DT+TAU*(VX1-UX1)*RELX
      Y2=Y1+UY1*DT+TAU*(VY1-UY1)*RELX
      Z=DSQRT(X2*X2+Y2*Y2)
C
C     CHECK IF PARTICLES HAVE IMPACTED ON WALLS BENEATH BOUNDARY LAYER
C
      IF(Z .LE. R) GO TO 30
      IF(Y2 .GE. 0.0 .AND. Y2 .LE. R) GO TO 30
      IF(Y2 .LE. (X2+1.414214*R)) GO TO 40
      IF(X2 .GE. 0.0 .AND. Z .GT. C) GO TO 50
      X1=X2
      Y1=Y2
      VX1=VX2
      VY1=VY2
      IF(X2 .GT. 0.0) GO TO 90
      GO TO 81
C     LOOP TO CHANGE DELTA TIME INTERVAL
   90 IF(J .NE. 1) GO TO 81
      DT=DT1
      T=(-DT/TAU)
      RELX=1.0-DEXP(T)
      J=0
      GO TO 81
C
C     CALCULATION OF EXACT DEPOSITION LOCATIONS
C
   30 XL(I)=0.0
      GO TO 69
   40 SLOEP=(Y2-Y1)/(X2-X1)
      XL(I)=1.414214*(((Y1-SLOEP*X1-1.414214*R)/(1-SLOEP))+.70711*R)
      IF(XL(I) .LT. 0.0) XL(I)=0.0
   69 CONTINUE
      N=IFIX(RUN-.9)
      M=N
      GO TO 54
   50 N=IFIX(RUN-1.9)
      M=N+1
   54 WRITE(6,51)
   51 FORMAT(1H1,15X,2HUX,18X,2HUY,18X,2HXL//)
      WRITE(6,52) (UX(I),UY(I),XL(I), I=1,M)
   52 FORMAT(1H0,3D20.8)
```

```
      WRITE(6,53)
   53 FORMAT(1H1)
      CALL DEPOST
      GO TO 5
      END
C SUBROUTINE TO CALCULATE THE DEPOSITION RATES AND LOCATIONS
      SUBROUTINE DEPOST
      COMMON UX(40),UY(40),XL(40),DELZ,N
      DOUBLE PRECISION AVUX,AVUY,AVEL,ANGL,ZL,FSC,DELZ,UX,UY,XL,ZLL,FLSC
      WRITE(6,5)
    5 FORMAT(1HO,20X,17HAVER DEP LOCATION,26X,13HDEP FLUX/CONC//)
      DO 15 K=1,N
      AVUX=(UX(K)+UX(K+1))/2.0
      AVUY=(UY(K)+UY(K+1))/2.0
      AVEL=DSQRT(AVUX*AVUX+AVUY*AVUY)
      ANGL=DATAN2(AVUY,AVUX)
      ZL=(XL(K)+XL(K+1))/2.0
      IF(ZL .LE. 0.0) GO TO 7
      FSC=AVEL*DELZ*DCOS(ANGL)/(XL(K+1)-XL(K))
      FLSC=DLOG10(FSC)
      ZLL=DLOG10(ZL)
      GO TO 9
    7 FSC=AVEL*DELZ*DCOS(ANGL)/(.00001)
      FLSC=DLOG10(FSC)
      ZLL=0.0
    9 WRITE(6,25) ZL,ZLL,FSC,FLSC
   25 FORMAT(1HO,D20.8,10X,F10.5,20X,D20.8,10X,F10.5)
   15 CONTINUE
      RETURN
      END
```

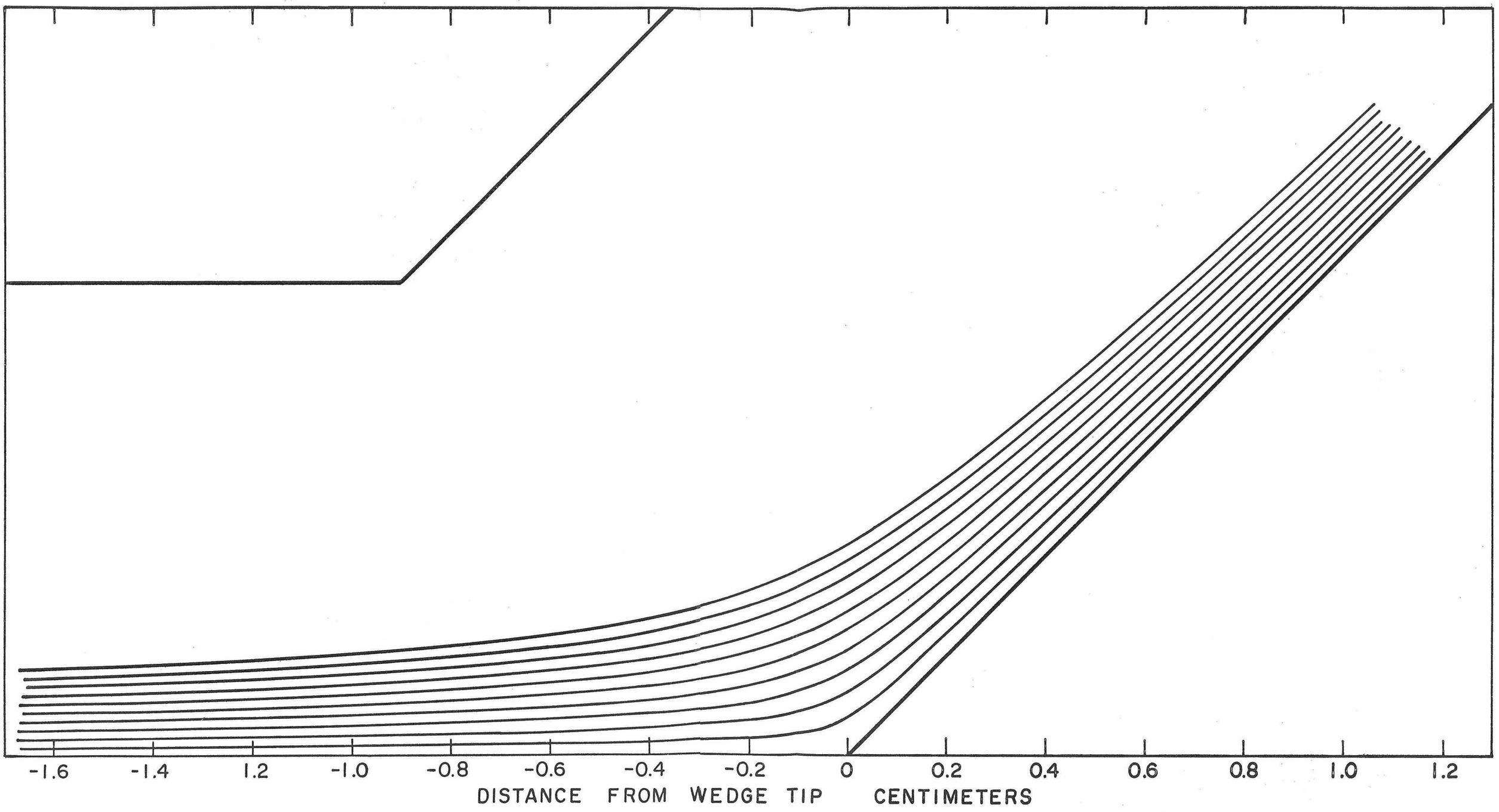

FIG. E1 STREAMLINES OF THE POTENTIAL FLOW AROUND A SYMMETRIC 90-DEGREE WEDGE

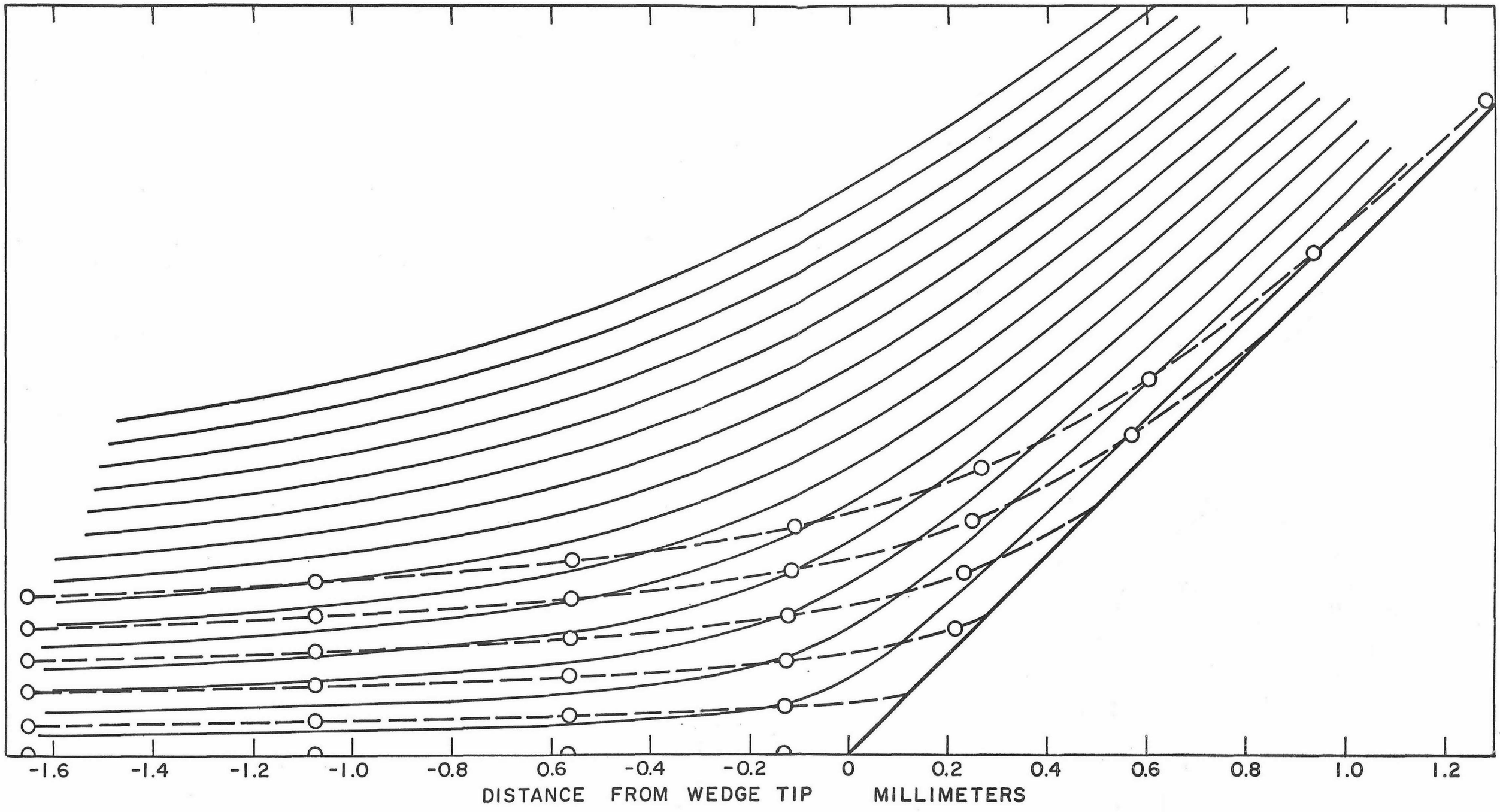

FIG. E2 STREAMLINES OF THE POTENTIAL FLOW AROUND A SYMMETRIC 90-DEGREE WEDGE AND INERTIAL DEPOSITION TRAJECTORIES OF AEROSOL PARTICLES